Online characterization of primary and secondary emissions of particulate matter and acidic molecules from a modern fleet of city buses

Liyuan Zhou[1,2#], Qianyun Liu[2,a#], Christian M. Salvador[3,b], Michael Le Breton[3,c], Mattias Hallquist[3], Jian Zhen Yu[4] and Chak K. Chan[1,2*], Åsa M. Hallquist[5*]

[1] Division of Physical Sciences and Engineering, King Abdullah University of Science and Technology, Thuwal, Saudi Arabia
[2] School of Energy and Environment, City University of Hong Kong, Hong Kong SAR, China
[3]Department of Chemistry and Molecular Biology, University of Gothenburg, Gothenburg, Sweden
[4]Division of Environment and Sustainability, Hong Kong University of Science and Technology, Hong Kong, China
[5]IVL Swedish Environmental Research Institute, Gothenburg, Sweden
[a]now at: RELX Science Center, Shenzhen RELX Tech. Co,. Ltd., Shenzhen, China
[b]now at: Environmental Sciences Division, Oak Ridge National Laboratory, Oak Ridge, TN 37830, USA
[c]now at: FEV Sverige AB, Gothenburg, Sweden

[#]The authors contribute equally.

Correspondence to: Åsa M Hallquist (asa.hallquist@ivl.se); Chak K. Chan (chak.chan@kaust.edu.sa)

Abstract. The potential impact of transitioning from conventional fossil fuel to a non-fossil fuel vehicle fleet was investigated by measuring primary emissions via extractive sampling of bus plumes and assessing secondary mass formation using a Gothenburg Potential Aerosol Mass (Go:PAM) reactor from 76 in-use transit buses. Online chemical characterization of gaseous and particulate emissions from these buses was conducted using a chemical ionization mass spectrometry (CIMS) with acetate as the reagent ion, coupled with a filter inlet for gases and aerosols (FIGAERO). Acetate reagent ion chemistry selectively ionizes acidic compounds, including organic and inorganic acids, as well as nitrated and sulfated organics. A significant reduction (48-98%) in fresh particle emissions was observed in buses utilizing compressed natural gas (CNG), biodiesels like rapeseed methyl ester (RME) and hydrotreated vegetable oil (HVO), as well as hybrid-electric HVO (HVO_{HEV}), compared to diesel (DSL) buses. However, secondary particle formation from photooxidation of emissions was substantial across all fuel types. The median ratio of particle mass emission factors of aged to fresh emissions increased in the following order: DSL buses at 4.0, HVO buses at 6.7, HVO_{HEV} buses at 10.5, RME buses at 10.8, and CNG buses at 84. Of the compounds that can be identified by CIMS, fresh gaseous emissions from all Euro V/EEV buses, regardless of fuel type, were dominated by nitrogen-containing compounds such as nitrous acid (HONO), nitric acid (HNO_3), and isocyanic acid (HNCO), alongside small monoacids (C_1-C_3). Notably, the emission of nitrogen-containing compounds was notably lower in Euro VI buses equipped with more advanced emission control technologies. Secondary gaseous organic acids correlated strongly with

gaseous HNO_3 signals (R^2= 0.85-0.99) in Go:PAM, but their moderate to weak correlations with post-photooxidation secondary particle mass suggest they are not reliable tracers for secondary organic aerosol formation from bus exhaust. Our study highlights that non-regulated compounds and secondary pollutant formation, not currently addressed in legislation, are crucial considerations in the evaluation of environmental impacts of future fuel and engine technology shifts.

1. Introduction

Air pollution remains a critical global issue, posing significant threats to both human health and the environment. Despite substantial progress in reducing emissions from major sources like industry, energy production, households, transportation, and agriculture, the worldwide achievement of air quality targets continues to be a daunting challenge. Notably, the road transport sector, particularly in urban environments, significantly contributes to the emissions of nitrogen oxides (NO_x) and particulate matter (PM), impacting the health of individuals in densely populated regions. In tandem with these concerns, efforts to combat climate change have spurred an increase in the adoption of renewable energy sources within the transportation sector. Biodiesel has risen as the most prevalent renewable fuel, followed by biogas and ED95 ethanol (Guerreiro et al., 2014). Moreover, numerous cities are progressively integrating hybrid-electric and electric vehicles into their public transport fleets, aiming to reduce emissions.

Emissions from vehicles, especially buses, exhibit considerable variability. They are influenced by fuel type, engine design, operational conditions, emission after-treatment technologies and maintenance (Pirjola et al., 2016; Zhao et al., 2018; Watne et al., 2018; Liu et al., 2019a; Zhou et al., 2020). While diesel (DSL) buses are common, there is an increasing trend towards the use of alternative fuels such as compressed natural gas (CNG), rapeseed methyl ester (RME), and hydrotreated vegetable oil (HVO). These alternative fuels offer several benefits, including reduced PM emissions, particularly soot, and lower levels of carbon monoxide (CO) and total hydrocarbons (THC) (Pflaum et al., 2010; Hassaneen et al., 2012; Liu et al., 2019a). However, the efficacy of RME and HVO in diminishing NO_x emissions can be inconsistent (Pirjola et al., 2016; Liu et al., 2019a); and CNG buses exhibit considerable variability in particle number (PN) emissions (Watne et al., 2018). In Sweden, approximately 23% of the fuel mix of the transport sector in 2020 comprised renewable fuels, with HVO accounting for over half of this proportion (Vourliotakis and Platsakis, 2022; Energimyndigheten, 2021). Emission control strategies, such as aftertreatment systems including diesel particulate filters (DPFs) and selective catalytic reduction (SCR) systems, have been implemented to mitigate pollutant emissions from vehicles. These systems have shown significant efficacy in reducing PM and NO_x emissions respectively, though their performance can vary under different operational conditions.

Accurately determining vehicle emission factors (EFs) is crucial for devising and implementing effective air quality policies (Fitzmaurice and Cohen, 2022). Methods such as chassis dynamometer tests, on-board measurements with portable emission measurement systems (PEMS), and on-road vehicle chasing experiments have been employed to assess emissions

from various types of vehicles (Kwak et al., 2014; Jezek et al., 2015; Pirjola et al., 2016). Chassis dynamometer tests offer high repeatability over standard drive cycles but may not reflect real-world driving conditions or fleet maintenance levels. There are also challenges in accurately replicating real-world dilution effects (Vogt et al., 2003; Kuittinen et al., 2021). On-board measurements with PEMS provide data under a wide range of operating conditions, yet like dynamometers, they may not realistically mimic ambient dilution processes (Giechaskiel et al., 2015; Wang et al., 2020). On-road vehicle chasing experiments involve following individual vehicles with a mobile laboratory to capture the exhaust plumes, providing insights into realistic dilution processes from the tailpipe to ambient air, though these experiments often require a test track to ensure traffic safety (Wang et al., 2020; Tong et al., 2022). All three methods are limited by small sample sizes, which constrain understanding of the real emission characteristics of vehicle fleets. Alternatively, roadside or near-road measurements provide the ability to monitor emissions from a large number of vehicles under actual driving conditions within a short timeframe (Hallquist et al., 2013; Watne et al., 2018; Liu et al., 2019a), which is particularly important for assessing exposure risks to pedestrians and bus passengers. However, this method is limited by its inability to monitor specific engines or operational conditions, such as varying engine speeds and loads. Integrating results from diverse methodologies would ideally yield a comprehensive understanding of emissions from vehicle transport systems.

In a prior study, we conducted roadside point measurements and reported EFs for general air pollutants such as PM, NO_x, CO, and THC from individual buses during stop-and-go operations at a bus stop in Gothenburg, Sweden (Liu et al., 2019a). Our findings showed that hybrid buses, when using their combustion engines to accelerate from a standstill at bus stops, tended to emit higher particle numbers (PN) than traditional DSL buses, likely due to their relatively smaller engines. Expanding on our prior findings, it is important to acknowledge that primary emissions are not the only way in which engine emissions impact air quality. Emissions from engine exhaust can contribute to secondary particles through oxidation of gas-phase species, primarily via functionalization reactions, yielding lower-volatility products (Hallquist et al., 2009; Kroll et al., 2009). Laboratory studies have demonstrated that secondary organic aerosols (SOA) produced from diluted vehicle exhaust frequently exceed the levels of primary organic aerosols (POA) in less than one day of atmospheric equivalent aging (Chirico et al., 2010; Nordin et al., 2013; Platt et al., 2013; Gordon et al., 2014b; Liu et al., 2015). Oxidation flow reactors (OFRs) enable the simulation of several days of atmospheric aging in a few minutes, with minimized wall effects compared to traditional smog chamber experiments (Palm et al., 2016; Bruns et al., 2015). OFRs have been extensively employed to assess the SOA formation potential of ambient air and emissions from diverse sources, including motor exhausts (Tkacik et al., 2014; Bruns et al., 2015; Simonen et al., 2017; Watne et al., 2018; Liu et al., 2019b; Kuittinen et al., 2021; Zhou et al., 2021; Liao et al., 2021a; Yao et al., 2022). In real-world traffic scenarios, the rapid response capabilities and convenient deployment of OFRs, coupled with roadside point measurements, provide a robust method for evaluating emissions from a significant number of vehicles. This approach effectively captures the considerable variability among individual vehicles within a fleet, offering a comprehensive view of emissions under actual driving conditions (Watne et al., 2018; Zhou et al., 2021), although it may not

encompass as extensive a range of engine operations as setups that integrate OFRs with chassis dynamometer tests (Kuittinen et al., 2021).

Primary emissions can also be oxidized to higher-volatility products through fragmentation reactions, potentially producing carboxylic acids (Friedman et al., 2017). Engine exhaust is a recognized primary source of organic and inorganic acids in urban environments (Kawamura et al., 1985; Kawamura and Kaplan, 1987; Kirchstetter et al., 1996; Wentzell et al., 2013; Friedman et al., 2017). Monocarboxylic acids are produced by both diesel and spark-ignited engines (Zervas et al., 2001b; Crisp et al., 2014; Zervas et al., 2001a; Kawamura et al., 1985). Recent studies have identified gaseous dicarboxylic acids in diesel exhaust (Arnold et al., 2012), compounds likely linked to the nucleation and growth of particles (Zhang et al., 2004; Pirjola et al., 2015). Additionally, inorganic acids such as nitric (HNO_3) and nitrous (HONO) acids, along with isocyanic acid (HNCO)—implicated in serious health issues like atherosclerosis, cataracts, and rheumatoid arthritis through carbamylation reactions—have been identified in both diesel and gasoline exhausts (Wang et al., 2007; Roberts et al., 2011; Wentzell et al., 2013; Brady et al., 2014; Link et al., 2016; Li et al., 2021). However, the secondary production of organic acid from engine exhaust remains poorly characterized; and it may significantly contribute to the overall organic acid budget and help explain discrepancies between models and measurements (Paulot et al., 2011; Millet et al., 2015; Yuan et al., 2015). Furthermore, the impacts of evolving fuel and engine technologies on emissions have not been comprehensively assessed. Recent advancements in analytical techniques now enable simultaneous, high-resolution online measurements of both gas and particle phase acidic species. This is facilitated by high-resolution time-of-flight chemical ionization mass spectrometry (HR-ToF-CIMS) using acetate as the reagent ion, coupled with a filter inlet for gases and aerosols (FIGAERO) (Le Breton et al., 2019; Friedman et al., 2017; Lopez-Hilfiker et al., 2014).

In this study, we employed the OFR Gothenburg Potential Aerosol Mass Reactor (Go:PAM) along with roadside point measurements to capture emissions from a diverse array of fuel types and engine technologies in in-use transit buses. We present findings on the photochemical aging of emissions from a modern fleet operating on diesel (DSL) and the latest generation of alternative fuels, including compressed natural gas (CNG), rapeseed methyl ester (RME), and hydrotreated vegetable oil (HVO). Our study aims to compare the secondary production of PM from individual buses in real traffic scenarios to their primary PM emissions, examining the impact of fuel type, engine technology, and photochemical age. Furthermore, both fresh and aged emissions of gas and particle phases are characterized using HR-ToF-CIMS, providing a comprehensive understanding of the emissions profile and their environmental implications.

2. Methods

2.1 Emission measurements

Roadside measurements were conducted at a designated urban bus stop, featuring a bus-only lane, in Gothenburg, Sweden. (Supporting information (SI), Figure S1). The sampling occurred from March 2nd to 12th, 2016, with the average temperature during this period recorded at approximately 3.9°C. Extractive sampling of individual bus plumes in real traffic was used to characterize emissions, adhering to the method outlined by Hallquist et al. (2013). Air was continuously drawn through a cord-reinforced flexible conductive hose to the instruments housed within a nearby container. Additional details of the experimental conditions are available in our prior publication by Liu et al. (2019a). The primary focus of this study was to utilize the OFR Go:PAM and the HR-ToF-CIMS to explore the potential for secondary pollutant formation and to conduct a detailed chemical characterization of both gas and particle phase compounds. An experimental schematic of the roadside sampling is shown in Figure S2. Briefly, the emissions from passing bus plumes were characterized as they accelerated from standstill at the bus stop. A camera was positioned at the roadside to capture bus plate numbers, facilitating bus identification and enabling the collection of specific information on each bus, including fuel type, engine technology, and exhaust after-treatment systems. The effective identification of emissions from individual buses was achieved by employing CO_2 as a tracer, as delineated by Hak et al. (2009). The concentration of CO_2 was measured with a non-dispersive infrared gas analyzer (LI-840A, time resolution 1 Hz). NO and NO_x were measured with two separate chemiluminescent analyzers (Thermo Scientific™ Model 42i NO-NO_2-NO_x Analyzer). In addition, specific gaseous compounds like CO, NO, and THC, were measured using a remote sensing device (AccuScan RSD 3000, Environmental System Products Inc.). Particle emissions were characterized using a high time resolution engine exhaust particle sizer spectrometer (EEPS, Model 3090 TSI Inc., time resolution 10 Hz) across a size range of 5.6-560 nm. Due to the lack of detailed knowledge about the chemical composition of the emitted particles, particle mass calculations were based on the assumption of spherical particles of unit density.

The HR-ToF-CIMS coupled with a FIGAERO was used to derive chemical information of both gas and particle phase species. A detailed description of the configuration of the instrument can be found elsewhere (Aljawhary et al., 2013; Lopez-Hilfiker et al., 2014; Le Breton et al., 2018; Le Breton et al., 2019). Acetate, employed as the reagent ion, was generated using an acetic anhydride permeation source through a ^{210}Po ion source (^{210}Po inline ionizer, NRD inc, Static Solutions Limited). In the ion-molecular reaction (IMR) chamber, the gaseous sampling flow interacted with the reagent ions, leading to the ionization of target molecules. The dual inlets of the FIGAERO enable simultaneous gas phase sampling directly into the IMR and particle sample collection on a PTFE filter for the duration of the plume via a separate inlet. The duration of the target plume for particle collection was indicated by particle number (PN) concentration measured by the EEPS. Once the PN concentration reduced to undistinguishable at background levels, the filter was automatically positioned to allow the collected particles to be evaporated into the IMR. The nitrogen flow over the filter was incrementally heated from room temperature to 200°C within 5 minutes and then maintained at this maximum temperature for 8 minutes, ensuring complete desorption of mass from the filter, followed by analysis via HR-ToF-CIMS. Perfluoropentanoic acid (PFPA), a reliable high mass calibrant, was injected into the CIMS inlet during the sampling period (Le Breton et al., 2019). Mass spectra were calibrated using known masses (m/z), accurate within 4 ppm: O_2-, CNO-, $C_3H_5O_3$-, $C_2F_3O_3$-, $C_5F_9O_2$-, $C_{10}F_{18}O_4$-, covering a range of 32-526 m/z (more details

can be found in SI). The data were acquired at 1 s time resolution. To estimate absolute EFs, a conversion of the CIMS signal to concentration using a sensitivity factor is necessary. Based on the method of Lopez-Hilfiker et al. (2015), the maximum sensitivity was determined to be 20 Hz ppt^{-1}, which falls within previously reported ranges (Mohr et al., 2017). Using this maximum sensitivity provides a lower-limit estimate of EFs for all oxygenated volatile organic compounds (Zhou et al., 2021). The assumption on sensitivity did not affect the comparative analysis of EFs with respect to different fuel types.

The EFs of constituents per kilogram of fuel burnt were calculated by relating the concentration change of a specific compound in the diluted exhaust plume to the change in CO_2 concentration. CO_2 served as a tracer for exhaust gas dilution, relative to background concentration (Janhäll and Hallquist, 2005; Hak et al., 2009; Hallquist et al., 2013; Watne et al., 2018). Assumptions were made for complete combustion and carbon contents of 86.1, 77.3, 70.5, and 69.2% for DSL, RME, HVO, and CNG, respectively, were assumed (Edwards et al., 2004). Further methodological details are elaborated in Liu et al. (2019a). A more comprehensive description of the EF calculations is provided in the Supporting Information.

2.2 Oxidation flow reactor setup

The OFR Go:PAM was utilized for photochemical aging of emissions from individual buses to investigate the potential for secondary pollutant formation. The comprehensive description and operational protocols of the Go:PAM have been detailed previously (Watne et al., 2018; Zhou et al., 2021). Briefly, the Go:PAM is a 6.1 L continuous-flow quartz glass flow reactor with input flows such that the median residence time is approximately 37s. The reactor is equipped with two Philips TUV 30 W fluorescent lamps (λ= 254 nm) and enclosed by reflective and polished aluminium mirrors to ensure a homogeneous photon field. The UV lamps generate OH radicals through the photolysis of O_3 in the presence of water vapor. The relative humidity (RH) within the reactor was around 60 - 80%. The O_3 concentration inside the Go:PAM was measured using an ozone monitor (2B technology, model 205 dual beam ozone monitor) at around 880 ppb prior to the introduction of vehicle exhaust. Particle wall losses in the Go:PAM were corrected using size-dependent transmission efficiency (Watne et al., 2018). The OH exposure (OH_{exp}) inside the Go:PAM was calibrated offline using sulfur dioxide (SO_2), following methodologies established in previous studies (Lambe et al., 2011; Kang et al., 2007), with additional details provided in the SI. During on-road measurements, the OH_{exp} may be significantly influenced by the OH reactivity (i.e., CO and HC) and titration of O_3 by NO in the plumes, which varied between vehicles. Thus, the OH reactivity was estimated for each bus passage using the maximum NO_x, CO and HC concentrations in the Go:PAM, along with corresponding water and ozone levels (Watne et al., 2018; Zhou et al., 2021). Employing the maximum concentrations of these OH- or O_3-consuming species represents a minimum estimate of OH_{exp} in our calculations. The flow-design incorporated in the Go:PAM enables investigation of transient phenomena, such as passing plumes. It also works at relatively low ozone concentrations (less than 1 ppm), limiting reactions of other potential oxidants such as O_3, NO_3, or O^1D (Zhou et al., 2021).

3. Results and discussion

3.1 Fresh and aged PM emissions from buses

The aged PM emissions ($EF_{PM:aged}$) of 133 plumes from a diverse set of buses, including 16 diesel (DSL), 11 compressed natural gas (CNG), 20 rapeseed methyl ester (RME), 20 hydrotreated vegetable oil (HVO) and 9 hybrid-electric HVO (HVO_{HEV}) buses, were investigated using Go:PAM. The corresponding average fresh PM emissions ($EF_{PM:Fresh}$) for these 76 buses were measured during several sequential days (Figure S2). These buses were a subset of the 234 buses described in our previous study (Liu et al., 2019a), and represent data corresponding to available Go:PAM measurements. A comprehensive discussion on the full data set for fresh condition is available in Liu et al. (2019a). Figure 1 shows the average $EF_{PM:Fresh}$ and $EF_{PM:aged}$ with respect to fuel type. Among the buses, Euro V DSL models had the highest median $EF_{PM:Fresh}$, $^{Md}EF_{PM:Fresh}$ (represented by the horizontal yellow lines), of 208 mg kg-fuel^{-1}, followed by HVO_{HEV}, RME and HVO buses with $^{Md}EF_{PM:Fresh}$ of 109, 74 and 62 mg kg-fuel^{-1} respectively. CNG buses and HVO_{HEV} buses equipped with a DPF under Euro VI standards exhibited the lowest $^{Md}EF_{PM:Fresh}$, with over half of these buses exhibiting $EF_{PM:Fresh}$ below the detection limit (<4.3 mg kg-fuel^{-1}). Except for HVO_{HEV} buses with a DPF, which was limited to a small tested number, all other bus types in this subset had $^{Md}EF_{PM:Fresh}$ comparable to those of the full data set in Liu et al. (2019a), within ±30% and following the same rank order. The average EFs of fresh and aged particle emissions and general gaseous pollutants for individual buses are given in Table 1.

After photooxidation in Go:PAM, particle mass increased markedly, with half of the individual buses showing average $EF_{PM:aged}$ more than eight times their average $EF_{PM:Fresh}$. For all Euro V/ EEV buses, the median $EF_{PM:aged}$, $^{Md}EF_{PM:aged}$ (represented by the horizontal blue lines), was highest for DSL buses of 749 mg kg-fuel^{-1} followed by a descending order of RME (655)> CNG (645) > HVO (543) > HVO_{HEV} (509). Despite low $EF_{PM:Fresh}$, CNG buses produced substantial secondary particle mass. The DPF, proven effective in earlier studies (Martinet et al., 2017; Preble et al., 2015; May et al., 2014), efficiently reduced primary particle emissions from DSL Euro III and HVO_{HEV} Euro VI buses. However, these bus types, even with DPFs, exhibited higher $EF_{PM:aged}$ than those using the same fuels but without DPFs (Euro V), albeit the number of tested buses with DPFs was limited. The variance in median $EF_{PM:aged}$ among different fuel types was less pronounced compared to $EF_{PM:Fresh}$, suggesting the presence of significant non-fuel-dependent precursor sources, such as lubrication oils and/or fuel additives (Watne et al., 2018; Le Breton et al., 2019).

Figure 2 shows the bus average $EF_{PM:Fresh}$ vs the corresponding $EF_{PM:aged}$ for individual bus passages, where the average $EF_{PM:aged}$ for each bus is indicated by a solid horizontal line. This analysis focuses on Euro V/EEV buses to ensure a sufficient number of buses in the comparison, while buses from other Euro classes were not included due to their limited numbers. The median ratio of $EF_{PM:aged}$ to $EF_{PM:Fresh}$ was highest for CNG buses (84), followed by RME (10.8), HVO_{HEV} (10.5), HVO (6.7) and DSL(4.0) buses. Buses equipped with DPFs, such as DSL Euro III and HVO_{HEV} Euro VI (not included in Figure 2), exhibited a median ratio exceeding 50. $EF_{PM:aged}$ exhibited notable variation between passages of the same bus, likely

attributable to emission variability between passages and different dilution levels for plumes prior to sampling into the Go:PAM. This is illustrated in Figure 2b, where $EF_{PM:Fresh}$ and $EF_{PM:aged}$ are presented as a function of the dilution level, indicated by the integrated CO_2 area. Generally, a higher integrated CO_2 area suggests a more concentrated plume, leading to increased external OH and O_3 reactivity, which in turn reduces the concentration of OH radicals available in the Go:PAM for precursor oxidation (Emanuelsson et al., 2013; Watne et al., 2018). Some buses displayed primary emissions too dilute for detection (markers located to the left in Figure 2b) but still exhibited non-negligible $EF_{PM:aged}$ after oxidation. To further examine the effects of simulated atmospheric oxidation in the Go:PAM, an estimated minimum OH_{exp} was calculated for each plume by incorporating the OH reactivities of CO and HC and the titration of O_3 with NO, following methodologies from Watne et al. (2018) and Zhou et al. (2021). For all plumes, OH_{exp} varied between 1.1×10^{9} to 4.6×10^{11} molecules cm^{-3} s. The $EF_{PM:aged}$ for some buses, for example, the DSL and HVO located to the right in Figure 2c, increased with increasing OH_{exp}. However, due to potential large differences in the chemical composition of emissions across different passages of the same bus, where some species are more prone to forming secondary particle mass even at lower OH_{exp}, the OH_{exp} dependent $EF_{PM:aged}$ for other buses was less pronounced.

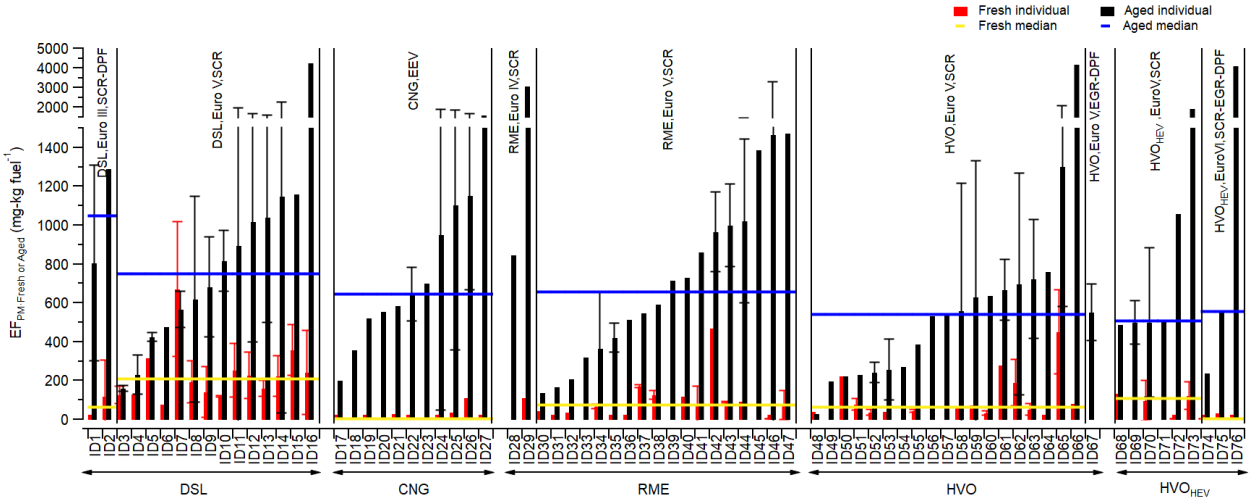

Figure 1. $EF_{PM:Fresh}$ (red bar) and $EF_{PM:aged}$ (black bar) with respect to fuel class: DSL (diesel, ID_1-ID_{16}), CNG (compressed natural gas, ID_{17}-ID_{27}), RME (rapeseed methyl ester, ID_{28}-ID_{47}), HVO (rapeseed methyl ester, ID_{48}-ID_{67}) and HVO_{HEV} (hybrid-electric HVO, ID_{68}-ID_{76}) buses. Median values for $EF_{PM:Fresh}$ ($^{Md}EF_{PM:Fresh}$) and $EF_{PM:aged}$ ($^{Md}EF_{PM:aged}$) are indicated by horizontal yellow and blue lines, respectively. The information on engine technology and exhaust after-treatment systems is also shown. Given errors represent the standard deviation (1σ).

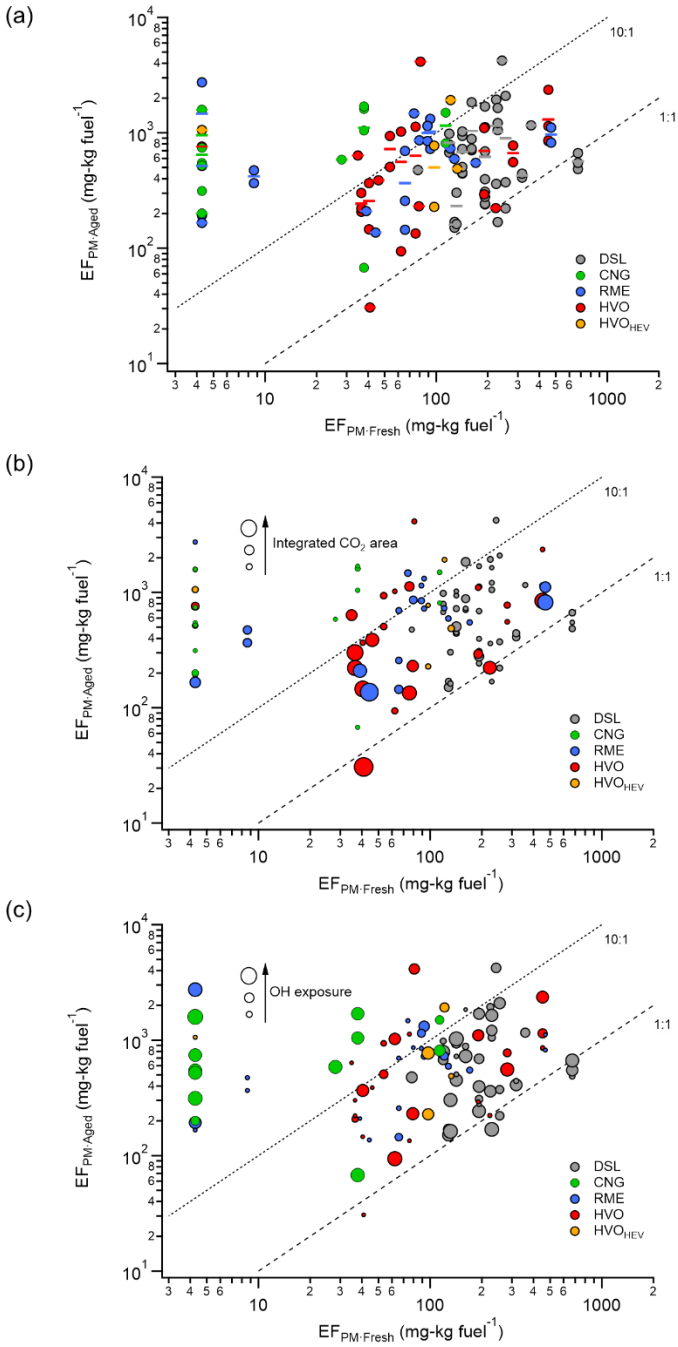

253

254

255 Figure 2. $EF_{PM:aged}$ vs average $EF_{PM:Fresh}$ for all the studied bus passages (Euro V) with respect to fuel type (a) and as a function
256 of integrated CO_2 area (b) and OH exposure (OH_{exp}) (c). The dashed lines denote the 10:1 and 1:1 $EF_{PM:aged}$: $EF_{PM:Fresh}$ ratios,
257 and the solid lines in (a) represent bus averages. One may note that the buses with $EF_{PM:Fresh}$ values below detection limit were

set to 4.3 mg kg-fuel^{-1}. Abbreviations: DSL (diesel), CNG (compressed natural gas), RME (rapeseed methyl ester), HVO (hydrotreated vegetable oil), HVO_{HEV} (hybrid-electric HVO).

Table 1. Average particle and gaseous EFs of individual buses for fresh emissions and average EF_{PM} for aged emissions[a].

Bus ID	Fuel[c]	Euro standard	Exhaust after-treatment system[d]	$EF_{PM:Fresh}$ (mg kg_{fuel}^{-1})	$EF_{PN:Fresh}$ (10^{14}# kg_{fuel}^{-1})	EF_{CO} (g kg_{fuel}^{-1})	EF_{THC} (g kg_{fuel}^{-1})	EF_{NOx} (g kg_{fuel}^{-1})	$EF_{PM:Aged}$ (mg kg_{fuel}^{-1})
1	DSL	III	SCR, DPF	4.3	0.41	3.9±11	1.5±2.9	10±3.2	810±510
2	DSL	III	SCR, DPF	120±190	34±61	2.7±7	1.7±3.7	11±5	1300
3	DSL	V	SCR	130±45	3.3±1.3	17±18	0.35±1.3	3.9±3.7	160±13
4	DSL	V	SCR	130	3.6	20±22	1.5±3.6	4.7±7.2	230±100
5	DSL	V	SCR	320	5.9	20±28	2±3.5	9.7±7	430±23
6	DSL	V	SCR	78	1.6	20±21	2.7±5.6	13±12	480
7	DSL	V	SCR	670±350	10±6.8	42±44	2.3±3.7	6.8±5	570±92
8	DSL	V	SCR	190±110	6.5±3	14±21	0.75±1.7	12±5.1	620±530
9	DSL	V	SCR	140±130	4.3±2.6	9.8±14	1±1.5	15±13	680±260
10	DSL	V	SCR	120±4.7	3.2±0.66	16±18	2.5±4.7	12±6.9	820±160
11	DSL	V	SCR	250±140	4.7±2.7	16±23	0.8±1.4	12±8.9	900±1000
12	DSL	V	SCR	230±120	5.1±1.5	16±26	2.6±4.6	12±9.9	1000±620
13	DSL	V	SCR	160±41	3.5±0.97	27±27	1.4±2.7	17±9.8	1000±540
14	DSL	V	SCR	220±110	5.2±1.3	12±17	2.6±4.1	11±7.4	1100±1100
15	DSL	V	SCR	360±130	6.8±4.2	21±25	1.2±3.3	5.7±4.4	1200
16	DSL	V	SCR	240±220	22±11	5.5±7.5	0.74±1.6	6.8±5.6	4200
17	CNG	EEV	-	4.3±0	0.41±0	n.a.	n.a.	4.8±1.7	200
18	CNG	EEV	-	n.a.	n.a.	n.a.	n.a.	11±4.9	360
19	CNG	EEV	-	4.3±0	0.41±0	n.a.	n.a.	4±3.8	520
20	CNG	EEV	-	n.a.	n.a.	n.a.	n.a.	15±17	560
21	CNG	EEV	-	28	1.3	n.a.	n.a.	2.2±0.93	590
22	CNG	EEV	-	4.3	0.41	n.a.	n.a.	1.8±1	650±140
23	CNG	EEV	-	n.a.	n.a.	n.a.	n.a.	3.2±0.53	700
24	CNG	EEV	-	4.3	0.41	n.a.	n.a.	6.9±1.4	950±900
25	CNG	EEV	-	38	11	n.a.	n.a.	7.3±5.3	1100±750
26	CNG	EEV	-	110	200	n.a.	n.a.	8.2±4.2	1200±480
27	CNG	EEV	-	4.3±0	0.41±0	n.a.	n.a.	6±1.8	1600
28	RME	IV	SCR	n.a.	n.a.	10±8.7	3.1±3	46±20	850
29	RME	IV	SCR	110	4.1	4.2±8.4	0.19±0.38	7.2±6.8	3000
30	RME	V	SCR	44	2.2	12±14	2.2±3.6	32±32	140
31	RME	V	SCR	4.3	0.41	7.4±7.1	0.075±0.17	13±5.1	170
32	RME	V	SCR	39	6.2	5.2±4.8	0.87±1.1	18±5.4	210
33	RME	V	SCR	n.a.	n.a.	0.24±0.54	0.24±0.39	10±3.3	320
34	RME	V	SCR	66±11	2.4±1	7±7.2	1.8±2.7	23±13	370±290
35	RME	V	SCR	8.6	0.96	4.9±3.6	0.59±0.73	20±5.1	420±75
36	RME	V	SCR	4.3	0.41	22±23	1.8±2	25±16	520
37	RME	V	SCR	170±7.7	6.4±1	34±35	0.016±0.043	19±10	550
38	RME	V	SCR	130±24	11±14	17±20	2±4	16±15	590
39	RME	V	SCR	n.a.	n.a.	1.2	0.64	21	720
40	RME	V	SCR	120	5.3	12±9.4	1.8±2.6	18±8.2	730
41	RME	V	SCR	80±95	4.2±2.9	8.8±17	0.72±0.87	25±5.7	860
42	RME	V	SCR	470	5.8	4.5±5.1	0.23±0.38	18±7.8	970±210
43	RME	V	SCR	89±2.3	2.6±0.16	5.4±9.4	0.68±1.9	28±17	1000±210
44	RME	V	SCR	92	1.6	14±19	1.8±3	23±17	1000±420
45	RME	V	SCR	n.a.	n.a.	37±26	5.8±3.6	14±6.3	1400
46	RME	V	SCR	4.3±0	0.41±0	9.6±14	0.89±1.4	28±8.4	1500±1800
47	RME	V	SCR	74±75	12±6	6.1±6.3	1.1±1.4	18±5.2	1500
48	HVO	V	SCR	41	1.5	8.4±2	0.14±0.31	10±0.4	31
49	HVO	V	SCR	n.a.	n.a.	5.8±8	0.7±0.62	13±10	200
50	HVO	V	SCR	220	6.6	8.3±9.1	0.91±0.97	13±8.6	220
51	HVO	V	SCR	79±31	2.6±0.74	7.8±5.8	0.41±0.59	12±8.2	230

52	HVO	V	SCR	37±13	1.9±0.65	4.8±5.5	0.64±0.82	20±3	240±51
53	HVO	V	SCR	40	2.5	2.1±3.4	0.0083±0.019	16±4.3	260±160
54	HVO	V	SCR	n.a.	n.a.	2.1±3	0.55±0.77	22	270
55	HVO	V	SCR	46±6.6	2.6±0.52	6.2±4.1	0.79±0.55	12±8.2	390
56	HVO	V	SCR	n.a.	n.a.	11±10	0.74±0.84	5.7	530
57	HVO	V	SCR	n.a.	n.a.	14±17	0.79±1.2	11±2.6	540
58	HVO	V	SCR	62	4.1	6.8±6.7	0.22±0.31	11±6.3	560±660
59	HVO	V	SCR	76	5.3	2.3±2	0.24±0.47	19±3.4	630±700
60	HVO	V	SCR	35±11	1.5±0.19	3.3±5	0.45±0.86	9.2±9	640
61	HVO	V	SCR	280	14	9.9±16	0.55±0.73	11±3.6	670±160
62	HVO	V	SCR	190±120	68±86	1.1±1.9	0.3±0.49	9.3±4.9	700±570
63	HVO	V	SCR	54±30	4.6±2.2	3.5±4.6	0.49±0.48	14±3.5	720±310
64	HVO	V	SCR	4.3	0.41	2.2±3.8	0.33±0.73	12±4.8	760
65	HVO	V	SCR	450±220	18±18	1.4±1.6	0.28±0.37	12±2.6	1300±720
66	HVO	V	SCR	81	11	0.88±0.93	0.28±0.25	13±6.5	4100
67	HVO	V	EGR, DPF	n.a.	n.a.	4.6±5.9	0.64±1.2	11±8.1	550±150
68	HVO_{HEV}	V	SCR	130	52	12±19	0.97±1.4	20±15	490
69	HVO_{HEV}	V	SCR	n.a.	n.a.	4.1±8.4	0.5±1.3	18±3.3	500±110
70	HVO_{HEV}	V	SCR	97±100	25±18	3.8±6.8	1.1±1.8	17±5.7	500±390
71	HVO_{HEV}	V	SCR	n.a.	n.a.	7.6±9.9	2.9±2.4	12±2.1	520
72	HVO_{HEV}	V	SCR	4.3±0	0.41±0	3.7±5.8	1±2.4	20±10	1100
73	HVO_{HEV}	V	SCR	120±72	8.9±2.9	1.2±1.7	0.18±0.26	17±7	1900
74	HVO_{HEV}	VI	SCR,EGR,DPF	4.3±0	0.41±0	4.7±11	2.2±4.7	7.2±8.5	240
75	HVO_{HEV}	VI	SCR,EGR,DPF	33	29	1.2±2.4	0.22±0.49	6.7±3.3	550
76	HVO_{HEV}	VI	SCR,EGR,DPF	4.3	0.41	10±9.2	1.5±2.3	8.8±8.7	4100

[a]Given errors represent the standard deviation (1σ).
[b]n.a., abbreviation for not available.
[c]DSL, CNG, RME, HVO and HVO_{HEV}, abbreviations for diesel, compressed natural gas, rapeseed methyl ester, hydrotreated vegetable oil, and hybrid-electric hydrotreated vegetable oil.
[d]SCR, DPF and EGR, abbreviations for selective catalytic reduction, diesel particulate filter and exhaust gas recirculation systems.

The secondary particle mass formed (ΔPM) was calculated as the difference between $EF_{PM:aged}$ for a plume and the average $EF_{PM:Fresh}$ for the corresponding individual bus. Figure 3 illustrates ΔPM as a function of OH_{exp} for the bus fleet in this study, which includes 40% DSL, 12.2% CNG, 20% RME, 20.8% HVO, and 7% HVO_{HEV}. The results were grouped based on OH_{exp}, spanning a range from 1.1×10^{9} to 4.6×10^{11} molecules cm^{-3} s. The results in this study are compared with those reported from a tunnel study (Tkacik et al., 2014), an urban roadside study of a mixed fleet in Hong Kong (Liu et al., 2019b), a depot study on rather modern types of city buses (Watne et al., 2018) and roadside measurements of a heavy-duty truck fleet in Gothenburg (Zhou et al., 2021). Laboratory OFR and chamber studies of middle-duty and heavy-duty diesel vehicles (Deng et al., 2017), diesel passenger cars (Chirico et al., 2010), a diesel engine (Jathar et al., 2017a), and gasoline vehicles (Gordon et al., 2014a; Platt et al., 2013) were also included for comparison.

The ΔPM from vehicle emissions is influenced by factors such as vehicle and fuel types, driving modes, and OH_{exp} during experiments (Gentner et al., 2017). Considering the variability of OH reactivity among vehicles and the consequently wide range of OH_{exp}, this study, along with Watne et al. (2018), categorizes ΔPM trend into OH_{exp} bins. The median ΔPM was approximately 400 mg $kg\text{-}fuel^{-1}$ at $OH_{exp} < 4.3 \times 10^{10}$ molecules cm^{-3} s (corresponding to 1 OH day, assuming an OH concentration of 1×10^{6} molecules cm^{-3} for 12 h per day) and was 364-495 mg $kg\text{-}fuel^{-1}$ at 1-5 OH days, reaching a maximum

of around 920 mg kg-fuel^{-1} at approximately 5-6 OH days for the bus fleet in this study. This peak value of ΔPM was lower than the approximately 3000 mg kg-fuel^{-1} at ~5-6 OH days observed in the depot measurements by Watne et al. (2018), a difference potentially due to variations in engine technology and fuel types used in the bus fleets. Notably, HVO was not used in the depot study, while some buses switched from RME to HVO prior to this study. The ΔPM peaked and then decreased at higher OH_{exp}, likely due to the transition from functionalization-dominated reactions and condensation at lower OH_{exp} to fragmentation reactions and evaporation dominance at higher OH_{exp} (Tkacik et al., 2014; Ortega et al., 2016). The ΔPM in this study was comparable to 855 mg kg-fuel^{-1} for a mixed fleet consisting of 44.1% gasoline, 41.3% diesel, and 14.6% LPG vehicles measured at an urban roadside in Hong Kong (Liu et al., 2019b). It was slightly higher than the ΔPM measured from a Euro VI dominated (more than 70%) heavy-duty truck fleet at an urban roadside in Gothenburg (Zhou et al., 2021), and from a fleet with over 80% light-duty gasoline vehicles in a Pittsburgh tunnel study (Tkacik et al., 2014). Additionally, the ΔPM in this study was consistent with that for middle-duty and heavy-duty diesel vehicles (Deng et al., 2017), diesel passenger cars (Chirico et al., 2010), and a diesel (or biodiesel)-fuelled engine under 50% load condition (Jathar et al., 2017a) (around 190-1133 mg kg-fuel^{-1}). However, the diesel (or biodiesel)-fuelled engine under idle conditions can produce significantly higher ΔPM (more than 5000 mg kg-fuel^{-1}), likely because engines at idle loads are less efficient at burning fuel, leading to higher emissions of unburnt gaseous combustion products (as precursors of secondary PM) (Nordin et al., 2013; Saliba et al., 2017; Jathar et al., 2017a). In contrast, experiments conducted for gasoline vehicles at relatively low photochemical ages (< 1 OH day) typically produced ΔPM lower than 70 mg kg-fuel^{-1} (Gordon et al., 2014a), except for a Euro 5 gasoline vehicle (340 mg kg-fuel^{-1}) operated with a New European Driving Cycle (Platt et al., 2013).

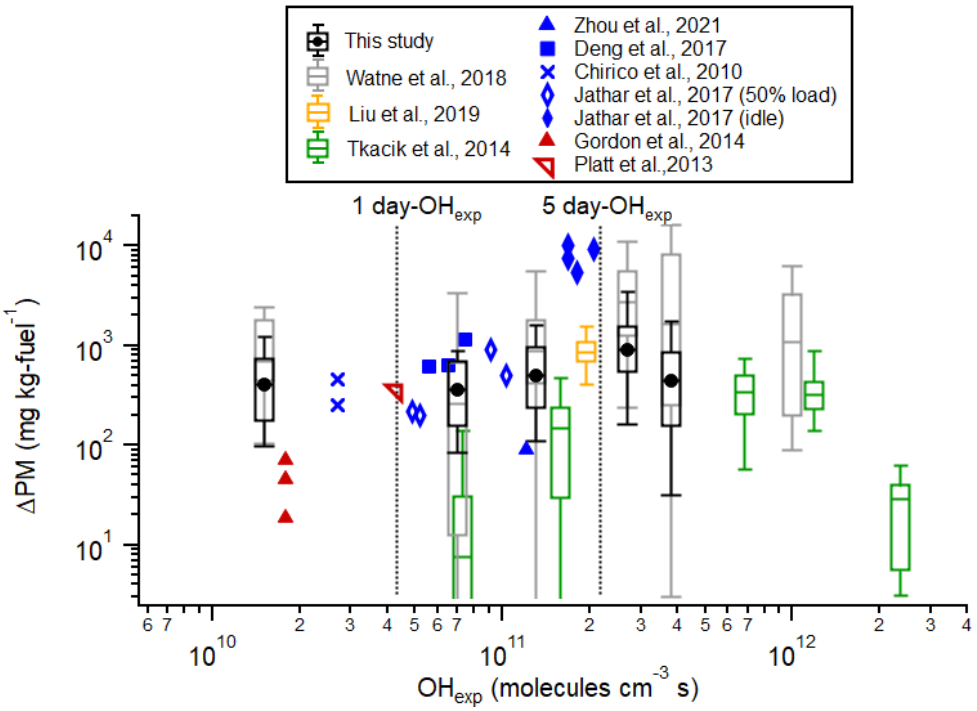

Figure 3. Secondary particle mass formed (ΔPM), calculated as $EF_{PM:aged}$ subtracted by the average $EF_{PM:Fresh}$, vs modeled OH exposure (OH_{exp}) for the bus fleet in this study and comparison with those reported for a tunnel study (Tkacik et al., 2014), a depot study (Watne et al., 2018), roadside measurements (Liu et al., 2019b; Zhou et al., 2021), middle-duty and heavy-duty diesel vehicles (Deng et al., 2017), diesel passenger cars (Chirico et al., 2010), a diesel engine (Jathar et al., 2017a), and gasoline vehicles (Gordon et al., 2014a; Platt et al., 2013). Dashed lines indicate 1- and 5-day OH_{exp} assuming an OH concentration of 1×10^6 molecules cm^{-3} 12 h per day (Watne et al., 2018). Note that ΔPM in this study, alongside those by Watne et al. (2018), Zhou et al. (2021) and Liu et al. (2019b), includes both secondary organic and inorganic aerosol, while ΔPM in research by Deng et al. (2017), Chirico et al. (2010), Jathar et al. (2017a), Gordon et al. (2014a), Platt et al. (2013) and Tkacik et al. (2014) pertains only to secondary organic aerosol mass.

3.2 Chemical characterization using CIMS

3.2.1 Fresh gaseous emissions

Figure 4 presents the median emission factors (^{Md}EFs) of acetate CIMS measured fresh gaseous emissions with respect to fuel type. The identities of the organic compounds detected by HR-ToF-CIMS are assigned based on knowledge of sensitivities of the ionization scheme and the expected compounds emitted from the buses. Plausible compounds are assigned from the

formulae, with a caveat that other isomers might contribute to the signal. These compounds were classified into nine families based on their molecular characteristics as outlined by Liu et al. (2017), with additional details provided in the SI. Among all Euro V/EEV buses, hybrid-electric HVO (HVO_{HEV}) buses exhibited the highest ^{Md}EF of CIMS measured fresh gaseous emissions (68 mg kg-fuel^{-1}), followed by DSL (42 mg kg-fuel^{-1}), RME (18 mg kg-fuel^{-1}), and CNG (16 mg kg-fuel^{-1}), while HVO had the lowest ^{Md}EF of 12 mg kg-fuel^{-1}. Nitrogen (N) -containing compounds (no sulfur) and monoacid families predominantly composed these fresh gaseous emissions. Compared to Euro V HVO_{HEV} buses, HVO_{HEV} buses equipped with exhaust gas recirculation (EGR) and DPF systems (Euro VI) demonstrated a significant reduction in ^{Md}EF (10 mg kg-fuel^{-1}), primarily due to decreased emissions of N-containing compounds, although the ^{Md}EF of other compound families were higher. In contrast, Zhou et al. (2021) reported significant reductions in both carboxylic acids and carbonyl compounds (by 94% on average), and acidic nitrogen-containing organic and inorganic species (79%) when transitioning from Euro V to Euro VI heavy-duty trucks. However, details on the types of exhaust after-treatment systems used in the trucks from such study are not specified. Moreover, this study utilized acetate as a different reagent ion for CIMS compared to the iodide used by Zhou et al. (2021). Table 2 lists the top 10 ^{Md}EFs of fresh gaseous compounds, contributing over 88% of total fresh gaseous emissions measured by CIMS for most bus types, except for Euro VI HVO_{HEV} (61%). The fresh gaseous emissions from all types of Euro V/EEV buses were primarily composed of nitrous acid (HONO) and nitric acid (HNO_3), with HONO being the most significant acidic emission. The ^{Md}EFs of HONO and HNO_3 generally align with values reported in the literature, ranging from approximately 7-250 mg kg-fuel^{-1} for HONO (Kurtenbach et al., 2001; Wentzell et al., 2013; Liao et al., 2020; Nakashima and Kondo, 2022) and around 4-14 mg kg-fuel^{-1} for HNO_3 (Wentzell et al., 2013). Acetic acid ($C_2H_4O_2$), formic acid (CH_2O_2), and isocyanic acid (HNCO) also exhibited relatively high ^{Md}EFs. The ^{Md}EFs of formic acid for all Euro V/EEV bus types (0.02-1.97 mg kg-fuel^{-1}) were consistent with those from a light-duty gasoline fleet (0.57−0.94 mg kg-fuel^{-1}) reported by Crisp et al. (2014). The ^{Md}EFs of acetic acid ranged from 1.23 to 4.84 mg kg-fuel^{-1}, falling between values for gasoline vehicles (0.78 mg kg-fuel^{-1}) and diesel buses (approximately 12-23 mg kg-fuel^{-1}) (Li et al., 2021). Isocyanic acid, likely an intermediate product of the thermal degradation of urea in SCR systems without sufficient hydrolysis (Bernhard et al., 2012), was detected in emissions from all bus types, with ^{Md}EFs of 0.08-14.74 mg kg-fuel^{-1}. These values are slightly lower than those from a non-road diesel engine (31-56 mg kg-fuel^{-1}) reported by Jathar et al. (2017b), but align well with SCR-equipped diesel vehicles tested by Suarez-Bertoa and Astorga (2016) (1.3-9.7 mg kg-fuel^{-1}) and a diesel engine with a diesel oxidation catalyst (DOC) (Wentzell et al., 2013) (0.21-3.96 mg kg-fuel^{-1}). Among all Euro V/EEV buses, HVO_{HEV} buses showed the highest emissions of HNCO, potentially attributed to cold engine conditions since the combustion engine does not operate continuously. Notably, emissions of HNCO were significantly lowered and neither HONO nor HNO_3 were identified among the top 10 ^{Md}EFs for HVO_{HEV} buses equipped with EGR and DPF systems (Euro VI), suggesting that newer engine technologies incorporating EGR and DPF systems likely effective in reducing emissions of NO_x (Table 1) as well as HNCO, HONO and HNO_3. CH_4SO_3, potentially identified as methanesulfonic acid, was detected in the emissions from DSL and RME buses. Previous studies, such as those by Corrêa and Arbilla (2008), have shown that mercaptans, emitted from diesel and biodiesel exhausts, can transform under high NOx conditions into products including methanesulfonic acid. The presence of sulfur-

containing organic compounds in diesel fuel and lubricants, and their potential transformation upon combustion into various sulfuric derivatives, alongside the catalytic activity of engine converters, could also contribute to such findings. However, the detailed formation pathway of CH_4SO_3 in our study remains unknown.

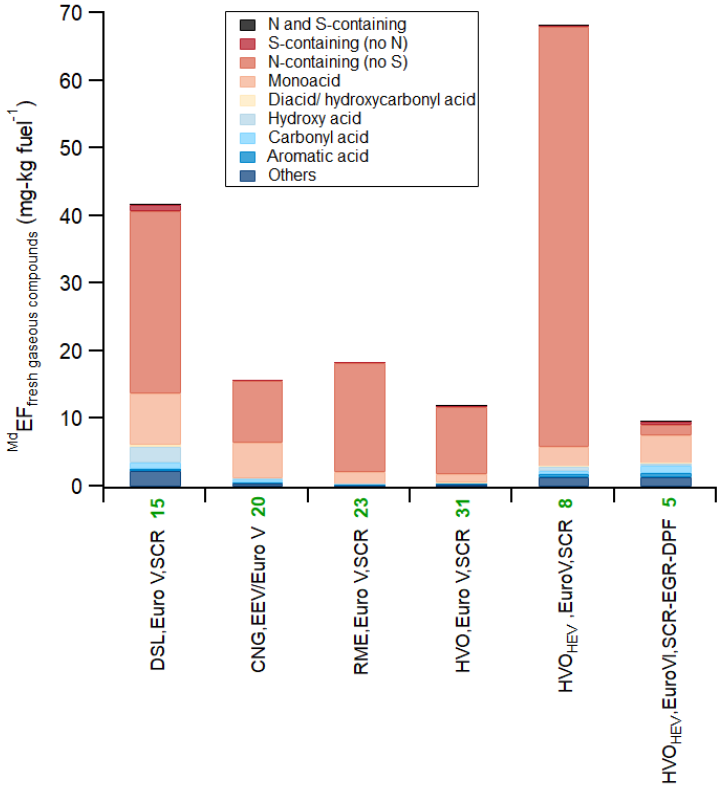

Figure 4. ^{Md}EFs of CIMS measured fresh gaseous emissions with respect to fuel class: DSL (diesel, 15), CNG (compressed natural gas, 20), RME (rapeseed methyl ester, 23), HVO (rapeseed methyl ester, 31) and HVO_{HEV} (hybrid-electric HVO, 13) buses. The number in bold green represents the number of buses examined.

Table 2. Summary of top 10 ^{Md}EFs of fresh gaseous compounds measured using HR-ToF-CIMS of DSL, CNG, RME, HVO and HVO_{HEV} buses[a] (color coded by different families shown in Figure 4).

DSL, Euro V, SCR		CNG, EEV/Euro V		RME, Euro V, SCR		HVO, Euro V, SCR		HVO_{HEV}, Euro V, SCR		HVO_{HEV}, Euro VI	
Species	^{Md}EF (mg kg_{fuel}^{-1})	Species	^{Md}EF (mg kg_{fuel}^{-1})	Species	^{Md}EF (mg kg_{fuel}^{-1})	Species	^{Md}EF (mg kg_{fuel}^{-1})	Species	^{Md}EF (mg kg_{fuel}^{-1})	Species	^{Md}EF (mg kg_{fuel}^{-1})
$HONO$	20.64	$HONO$	4.92	$HONO$	12.72	$HONO$	7.62	$HONO$	38.96	$C_3H_2O_2$	2.42
HNO_3	5.29	$C_2H_4O_2$	4.68	HNO_3	3.24	HNO_3	2.20	$HNCO$	14.74	$C_2H_4O_2$	1.23
$C_2H_4O_2$	4.84	HNO_3	3.48	$C_2H_4O_2$	1.23	$C_2H_4O_2$	1.23	HNO_3	7.89	$C_2H_2O_3$	0.62
CH_2O_2	1.97	$HNCO$	0.51	CH_2O_2	0.48	$C_3H_6O_3$	0.14	$C_2H_4O_2$	1.83	$C_8H_6O_4$	0.40
$C_3H_6O_3$	1.79	CH_2O_2	0.30	$HNCO$	0.15	$C_3H_2O_2$	0.09	CH_2O_2	0.45	$C_6H_5NO_2$	0.31
CH_4SO_3	0.71	$C_2H_2O_3$	0.25	$C_2H_2O_3$	0.05	$HNCO$	0.08	$C_3H_6O_3$	0.43	$HNCO$	0.27
$HNCO$	0.67	$C_3H_2O_2$	0.14	$C_5H_8O_3$	0.03	CH_2O_2	0.02	$C_3H_2O_2$	0.34	$C_3H_4O_5$	0.22
$C_3H_4O_5$	0.37	$C_3H_4O_2$	0.06	CH_4SO_3	0.02	$C_2H_2O_3$	0.02	$C_9H_{10}O_3$	0.16	$C_7H_6O_3$	0.20
$C_2H_2O_3$	0.31	$C_7H_6O_3$	0.05	$C_3H_4O_2$	0.02	$C_3H_4O_3$	0.02	$C_8H_6O_4$	0.12	$C_5H_8O_3$	0.17
$C_4H_6O_4$	0.22	$C_5H_8O_4$	0.05	$C_6H_6N_2O_2$	0.01	$C_4H_6O_4$	0.01	$C_5H_8O_3$	0.10	$H_4N_2O_2S$	0.16

[a]DSL, CNG, RME, HVO and HVO_{HEV}, abbreviations for diesel, compressed natural gas, rapeseed methyl ester, hydrotreated vegetable oil, and hybrid-electric hydrotreated vegetable oil.

3.2.2 Aged gaseous emissions

Secondary carboxylic acids were measured following exposure of the exhaust to OH radicals. Figure 5 shows the correlations between ion counts of the most abundant gas-phase organic acids and nitric acid (HNO_3) after oxidation in the Go:PAM. HNO_3 serves as an indicator of NO_x oxidation. Most acids exhibited both primary and secondary sources, except for dihydroxyacetic acid ($C_2H_4O_4$), which was only identified post-aging. The chemical characterization of the aged emissions was conducted on separate occasions using HR-ToF-CIMS, capturing a limited number of buses (N=19). When these buses were categorized by fuel type, the sample size for each category became smaller, constraining statistical comparison across different bus types. Nevertheless, we analyzed the relationship between various chemical species across all buses. Glycolic acid ($C_2H_4O_3$), dihydroxyacetic acid ($C_2H_4O_4$), pyruvic acid ($C_3H_4O_3$), malonic acid ($C_3H_4O_4$), lactic acid ($C_3H_6O_3$) and acetoacetic acid ($C_4H_6O_3$) showed high correlations (R^2= 0.85-0.99, Fig. 5a-f) with HNO_3 signals. In contrast, glutaric acid ($C_5H_8O_4$) and succinic acid ($C_4H_6O_4$) exhibited poorer correlations with HNO_3, suggesting different formation mechanisms for these two organic acids compared to the others mentioned. Notably, these two acids showed a strong correlation with each other (R^2= 0.97, Fig. 5i) and both belong to the diacid/hydroxycarbonyl acid families. It is important to note that many of these carboxylic acids can directly participate in secondary PM formation in the atmosphere in the presence of water vapor and a base such as ammonia (Chen et al., 2020; Huang et al., 2018; Hao et al., 2020). This process may significantly contribute to the overall secondary PM yield, reflecting a more complex interplay between gaseous emissions and particulate matter under atmospheric conditions. While most of these small organic acids correlated well with HNO_3, their correlations with $EF_{PM:aged}$ or ΔPM were

moderate to weak ($R^2 < 0.6$, Figure S5). This possibly indicates that the OH-driven formation of these carboxylic acids occurs on a different time scale compared to the production of organic aerosol (Friedman et al., 2017), at least in this Go:PAM experiment. This could also be due to different subsets of hydrocarbon precursors driving the production of organic acids and secondary particle mass. Similarly, Friedman et al. (2017) observed a lack of correlation between organic aerosol and gaseous organic acid concentrations downstream of the flow reactor from a diesel engine, indicating that organic acids may not be reliable tracers for secondary organic aerosol formation from diesel exhaust.

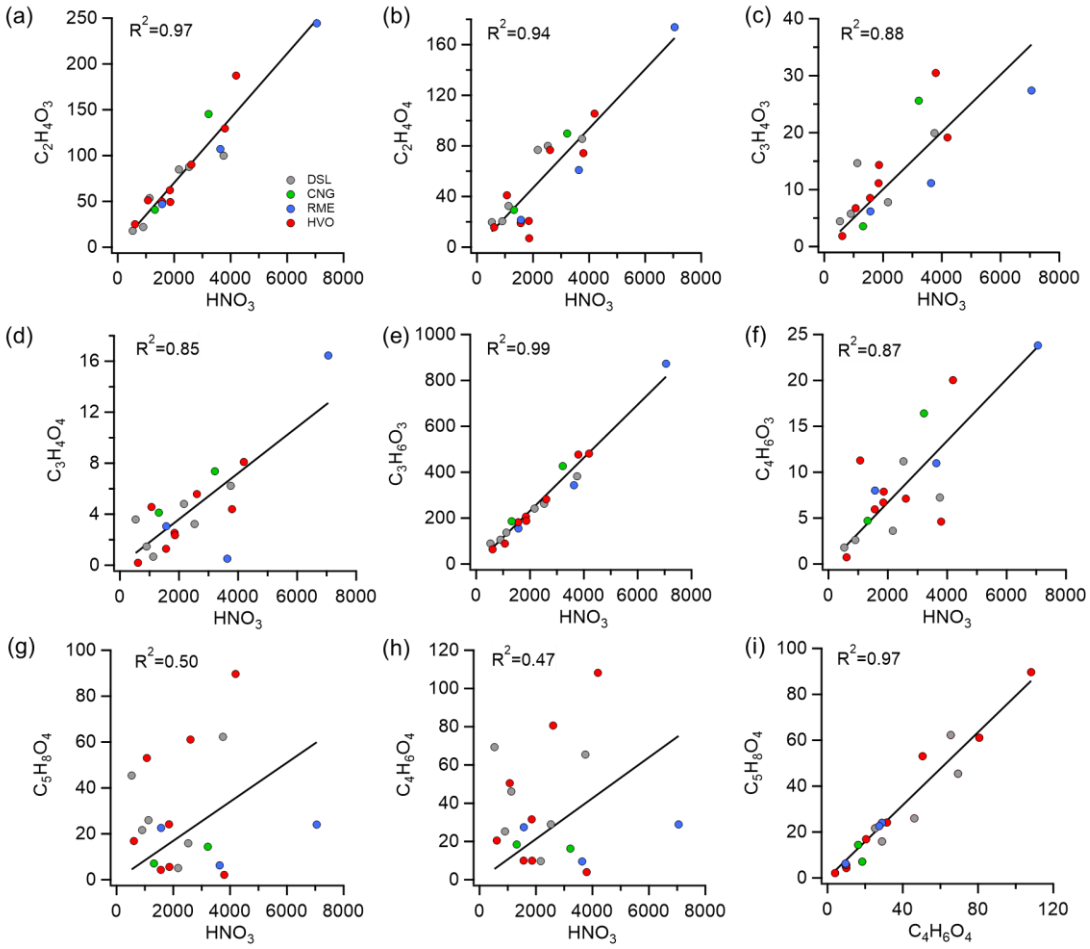

Figure 5. Correlations between ion counts of most abundant gas-phase organic acids and HNO_3 (a-h) and correlation between glutaric acid ($C_5H_8O_4$) and succinic acid ($C_4H_6O_4$) (i) from 19 buses after oxidation in the Go:PAM. Abbreviations: DSL (diesel), CNG (compressed natural gas), RME (rapeseed methyl ester), HVO (hydrotreated vegetable oil), HVO_{HEV} (hybrid-electric HVO).

3.2.3 Particulate emissions

Table 3 displays the top 10 EFs of fresh particle-phase compounds (EF_{fresh}), as characterized by the FIGAERO ToF-CIMS, alongside their respective aged EFs (EF_{aged}), for Euro V DSL and RME buses. These top 10 EF_{fresh} contributed to over 82% of the total fresh particulate emissions measured by CIMS. Fresh particulate emissions from DSL buses were predominantly composed of sulfuric acid (H_2SO_4) and nitric acid (HNO_3). Benzene/toluene oxidation products ($C_7H_4O_7$, C_7H_8O, $C_6H_5NO_3$, C_6H_5O, $C_7H_7NO_3$) also had relatively high EF_{fresh}, aligning with the findings in Le Breton et al. (2019). Similarly, high EF_{fresh} of HNO_3 (2.5 mg kg-fuel^{-1}) and H_2SO_4 (0.61 kg-fuel^{-1}) were observed for the RME bus. Additionally, fatty acids, known as main components of unburned rapeseed oil (Usmanov et al., 2015), such as $C_{18}H_{34}O_2$, $C_{14}H_{28}O_2$, $C_{18}H_{36}O_2$,$C_{16}H_{32}O_2$, and $C_{16}H_{30}O_2$, significantly contributed to the identified mass loadings from the RME bus. When comparing the percentage mass observed by CIMS for both DSL and RME fuels in fresh and aged exhaust plumes, the total emission factors measured by CIMS (EF_{CIMS}) were notably lower than the total emission factors measured by the EEPS (EF_{total}). This difference is expected due to the sensitivity of the acetate ionization scheme of CIMS, which efficiently detects oxygenated volatile organic compounds, particularly carboxylic acids and inorganic acids, but has low sensitivity towards hydrocarbons and cannot detect metallic ions and soot. The CIMS measured EF_{fresh} accounted for 10.4% and 5.9% of the fresh EF_{total} measured by the EEPS for DSL and RME, respectively. In aged exhaust, EF_{CIMS} represented a higher percentage of EF_{total} (25.8% for DSL and 17.9% for RME), likely because of an increased proportion of organics with acid groups.

Table 3. Summary of top 10 EF_{fresh} of PM contributing species with respective EF_{aged} in Euro V DSL and RME emissions.

DSL			RME		
Species	EF_{fresh} ($mg\ kg_{fuel}^{-1}$)	EF_{aged} ($mg\ kg_{fuel}^{-1}$)	Species	EF_{fresh} ($mg\ kg_{fuel}^{-1}$)	EF_{aged} ($mg\ kg_{fuel}^{-1}$)
H_2SO_4	4.8	6.8	HNO_3	2.5	45
HNO_3	3.2	50	$C_{18}H_{34}O_2$	1.2	0.81
$C_7H_4O_7$	1.8	3.8	H_2SO_4	0.61	0.68
HNCO	1.1	1.2	$C_{14}H_{28}O_2$	0.52	0.85
C_7H_8O	0.9	7.2	HNCO	0.45	0.089
$C_3H_6O_3$	0.6	23	$C_{18}H_{36}O_2$	0.32	0.046
$C_6H_5NO_3$	0.53	2.6	$C_{16}H_{32}O_2$	0.30	0.18
$C_4H_6O_5$	0.45	0.30	$C_6H_5O_2$	0.12	8.6
C_6H_5O	0.26	15.6	$C_4H_6O_4$	0.089	6.3
$C_7H_7NO_3$	0.15	4.6	$C_{16}H_{30}O_2$	0.081	0.012
EF_{total} measured by the EEPS	160.9	1289.8	EF_{total} measured by the EEPS	127.7	1320.6
EF_{CIMS}	16.8	320.1	EF_{CIMS}	7.5	237.2
EF_{CIMS}/EF_{total} (%)	10.4	25.8	EF_{CIMS}/EF_{total} (%)	5.9	17.9

4. Conclusion/ atmospheric implications

To address the challenges posed by increasing transportation needs, associated greenhouse gas emissions, and related climate change impacts, biofuels have been promoted as a low-carbon alternative to fossil fuels. In 2020, for the 27 Member States of the European Union, 93.2% of the total fuel supply for road transport was derived from fossil fuels, while 6.8% came from biofuels, with Sweden having the highest biofuel share at 23.2% (Vourliotakis and Platsakis, 2022). This study investigated renewable fuels like rapeseed methyl ester (RME), hydrotreated vegetable oil (HVO), and methane (when using biogas) in terms of primary emissions of pollutants and their secondary formation after photochemical aging. DSL buses without a DPF displayed the highest $EF_{PM:Fresh}$, whereas compressed natural gas (CNG) buses emitted the least, with a median $EF_{PM:Fresh}$ below the detection limit. Despite more than an order of magnitude difference in $EF_{PM:Fresh}$ among buses operated with various fuel types, we observed smaller variations in $EF_{PM:Aged}$, suggesting that secondary particle formation is likely influenced by substantial non-fuel-dependent precursor sources such as lubrication oils and/or fuel additives. Recognizing these sources is crucial for refining regulations on hydrocarbon emissions, which could notably enhance SOA control. The median ratios of aged to fresh particle mass emission factors, listed in ascending order, were for diesel (4.0), HVO (6.7), HVO_{HEV} (10.5), RME (10.8), and CNG buses (84), highlighting the significant yet often overlooked contributions of aged/photochemically processed emissions to urban air quality. Furthermore, Zhao et al. (2017) revealed a strongly nonlinear relationship between SOA formation from vehicle exhaust and the ratio of non-methane organic gas to NO_x ($NMOG:NO_x$). For instance, increasing the $NMOG:NO_x$ from 4 to 10 $ppbC/ppbNO_x$ increased the SOA yield from dilute gasoline vehicle exhaust by a factor of 8, underscoring the importance of integrated emission control policies for NO_x and organic gases for better manage SOA formation. While implementing regulations for secondary particle formation presents significant challenges, these are crucial for a thorough understanding of their impact on regional air quality and health. Our approach to measuring the maximum SOA formation potential—peaking at a photochemical age of approximately 5 equivalent days of atmospheric OH exposure—provides a possible semi-quantitative reference for comparing SOA formation potential across different studies. We acknowledge the limitations of this approach for direct regulatory application and emphasize the need for more precise and comprehensive research to develop a methodologically robust framework that stakeholders can agree upon for systematically assessing the impacts of vehicle on air quality and informing regulatory strategies.

It is important to note that the ambient temperature during this study was relatively low, which does not affect the EF comparison across different buses but should be aware of when comparing these results to studies conducted at significantly higher temperatures. Wang et al. (2017) noted lower particle number EFs in summer compared to winter, potentially due to increased nucleation or condensation at cooler temperatures. Temperature impacts on emissions are significant during cold starts when combustion is inefficient (Nam et al., 2010). Post-warm-up, soot mode particles show little temperature sensitivity (Ristimäki et al., 2005). Book et al. (2015) found inconsistent trends in particle emissions from DPF-equipped

diesel trucks across various temperatures and driving cycles, suggesting that more research is needed to understand the temperature effects on emissions from different bus types under varied operational conditions.

Non-regulated chemical species can also have serious negative impacts on air quality and human health. Organic and inorganic acids influence the pH of precipitation and will potentially contribute to acid deposition, affecting ecosystem health. Furthermore, there is a risk that some abatement systems might generate unintended compounds, such as HNCO from the thermal degradation of urea in SCR systems without sufficient hydrolysis. Additionally, Jathar et al. (2017b) observed substantial direct emissions of HNCO from diesel engines and estimated that ambient concentrations in Los Angeles could vary widely, ranging from 20 to 107 ppt depending on different parameterizations of diesel engine emissions. The persistence of HNCO in the atmosphere, particularly under dry conditions, poses significant health risks. It has been linked to severe outcomes including respiratory and cardiovascular disorders, atherosclerosis, cataracts, and rheumatoid arthritis (Leslie et al., 2019; Roberts et al., 2011). In our study, small monoacids (C_1-C_3) and nitrogen-containing compounds, such as nitrous acid (HONO), nitric acid (HNO_3), and HNCO, dominated the fresh gaseous emissions measured by acetate-CIMS for all Euro V/EEV buses regardless of fuel type, with HVO_{HEV} buses exhibiting the highest emissions. Notably, the emission levels of nitrogen-containing compounds were significantly lowered in Euro VI buses, equipped with advanced after-treatment systems that include EGR and DPF technologies in addition to SCR-only techniques. This indicates that transitioning to vehicles equipped with more advanced emission control technologies can be beneficial, even though these technologies may not be specifically designed to target emissions of HONO, HNO_3, and HNCO. Consequently, a detailed evaluation of the environmental and health effects of emerging engine and after-treatment technologies is highly desirable for future considerations. Overall, the extended online chemical characterization of in-use fleet emissions, utilizing advanced techniques like HR-ToF-CIMS, enables the identification of unregulated pollutants, which is crucial for more informed policy decisions and vehicle technology developments.

Data availability.

The data used in this publication are available to the community and can be accessed by request to the corresponding author.

Author contributions.

ÅMH, MLB and QL conducted the measurements. ÅMH designed the project, coordinated the measurements and together with MH and CKC supervised the study. LZ, QL, MLB, CMS and ÅMH carried out the data analysis. LZ, QL, JZY, MH, ÅMH and CKC prepared the manuscript. All co-authors contributed to the discussion and the interpretation of the results.

Competing interests.

The authors declare that they have no known competing financial interests or personal relationships that could have appeared to influence the work reported in this paper.

Acknowledgments.

This work was financed by VINNOVA, Sweden's Innovation Agency (2013-03058) and Formas (2020-1907) and was an initiative within the framework programme "Photochemical smog in China" financed by the Swedish Research Council (639-2013-6917). Chak K. Chan would like to acknowledge the support of the National Natural Science Foundation of China (project no. 41675117 and 41875142).

References

Aljawhary, D., Lee, A. K. Y., and Abbatt, J. P. D.: High-resolution chemical ionization mass spectrometry (ToF-CIMS): application to study SOA composition and processing, Atmospheric Measurement Techniques, 6, 3211-3224, 10.5194/amt-6-3211-2013, 2013.

Arnold, F., Pirjola, L., Ronkko, T., Reichl, U., Schlager, H., Lahde, T., Heikkila, J., and Keskinen, J.: First online measurements of sulfuric acid gas in modern heavy-duty diesel engine exhaust: implications for nanoparticle formation, Environmental science & technology, 46, 11227-11234, 2012.

Bernhard, A. M., Peitz, D., Elsener, M., Wokaun, A., and Kröcher, O.: Hydrolysis and thermolysis of urea and its decomposition byproducts biuret, cyanuric acid and melamine over anatase TiO2, Applied Catalysis B: Environmental, 115, 129-137, 2012.

Book, E. K., Snow, R., Long, T., Fang, T., and Baldauf, R.: Temperature effects on particulate emissions from DPF-equipped diesel trucks operating on conventional and biodiesel fuels, Journal of the Air & Waste Management Association, 65, 751-758, 2015.

Brady, J. M., Crisp, T. A., Collier, S., Kuwayama, T., Forestieri, S. D., Perraud, V., Zhang, Q., Kleeman, M. J., Cappa, C. D., and Bertram, T. H.: Real-time emission factor measurements of isocyanic acid from light duty gasoline vehicles, Environ Sci Technol, 48, 11405-11412, 10.1021/es504354p, 2014.

Bruns, E., El Haddad, I., Keller, A., Klein, F., Kumar, N., Pieber, S., Corbin, J., Slowik, J., Brune, W., and Baltensperger, U.: Inter-comparison of laboratory smog chamber and flow reactor systems on organic aerosol yield and composition, Atmospheric Measurement Techniques, 8, 2315-2332, 2015.

Chen, L., Bao, Z., Wu, X., Li, K., Han, L., Zhao, X., Zhang, X., Wang, Z., Azzi, M., and Cen, K.: The effects of humidity and ammonia on the chemical composition of secondary aerosols from toluene/NOx photo-oxidation, Science of The Total Environment, 728, 138671, 2020.

Chirico, R., DeCarlo, P., Heringa, M., Tritscher, T., Richter, R., Prévôt, A., Dommen, J., Weingartner, E., Wehrle, G., and Gysel, M.: Impact of aftertreatment devices on primary emissions and secondary organic aerosol formation potential from in-use diesel vehicles: results from smog chamber experiments, Atmospheric Chemistry & Physics, 10, 11545-11563, 2010.

Corrêa, S. M., and Arbilla, G.: Mercaptans emissions in diesel and biodiesel exhaust, Atmospheric Environment, 42, 6721-6725, 2008.

Crisp, T. A., Brady, J. M., Cappa, C. D., Collier, S., Forestieri, S. D., Kleeman, M. J., Kuwayama, T., Lerner, B. M., Williams, E. J., and Zhang, Q.: On the primary emission of formic acid from light duty gasoline vehicles and ocean-going vessels, Atmospheric Environment, 98, 426-433, 2014.

Deng, W., Hu, Q., Liu, T., Wang, X., Zhang, Y., Song, W., Sun, Y., Bi, X., Yu, J., Yang, W., Huang, X., Zhang, Z., Huang, Z., He, Q., Mellouki, A., and George, C.: Primary particulate emissions and secondary organic aerosol (SOA) formation from idling diesel vehicle exhaust in China, Sci Total Environ, 593-594, 462-469, 10.1016/j.scitotenv.2017.03.088, 2017.

Edwards, R., Mahieu, V., Griesemann, J.-C., Larivé, J.-F., and Rickeard, D. J.: Well-to-wheels analysis of future automotive fuels and powertrains in the European context, SAE Technical Paper0148-7191, 2004.

Emanuelsson, E. U., Hallquist, M., Kristensen, K., Glasius, M., Bohn, B., Fuchs, H., Kammer, B., Kiendler-Scharr, A., Nehr, S., and Rubach, F.: Formation of anthropogenic secondary organic aerosol (SOA) and its influence on biogenic SOA properties, Atmospheric Chemistry and Physics, 13, 2837-2855, 2013.

Energimyndigheten: Energy in Sweden 2021 – An Overview, 2021.

Fitzmaurice, H. L., and Cohen, R. C.: A method for using stationary networks to observe long-term trends of on-road emission factors of primary aerosol from heavy-duty vehicles, Atmospheric Chemistry and Physics, 22, 15403-15411, 2022.

Friedman, B., Link, M. F., Fulgham, S. R., Brophy, P., Galang, A., Brune, W. H., Jathar, S. H., and Farmer, D. K.: Primary and Secondary Sources of Gas-Phase Organic Acids from Diesel Exhaust, Environ Sci Technol, 51, 10872-10880, 10.1021/acs.est.7b01169, 2017.

Gentner, D. R., Jathar, S. H., Gordon, T. D., Bahreini, R., Day, D. A., El Haddad, I., Hayes, P. L., Pieber, S. M., Platt, S. M., and de Gouw, J.: Review of urban secondary organic aerosol formation from gasoline and diesel motor vehicle emissions, Environmental science & technology, 51, 1074-1093, 2017.

Ghadimi, S., Zhu, H., Durbin, T. D., Cocker III, D. R., and Karavalakis, G.: Exceedances of Secondary Aerosol Formation from In-Use Natural Gas Heavy-Duty Vehicles Compared to Diesel Heavy-Duty Vehicles, Environmental Science & Technology, 57, 19979-19989, 2023.
Giechaskiel, B., Riccobono, F., Vlachos, T., Mendoza-Villafuerte, P., Suarez-Bertoa, R., Fontaras, G., Bonnel, P., and Weiss, M.: Vehicle emission factors of solid nanoparticles in the laboratory and on the road using portable emission measurement systems (PEMS), Frontiers in Environmental Science, 3, 82, 2015.
Gordon, T. D., Presto, A. A., May, A. A., Nguyen, N. T., Lipsky, E. M., Donahue, N. M., Gutierrez, A., Zhang, M., Maddox, C., Rieger, P., Chattopadhyay, S., Maldonado, H., Maricq, M. M., and Robinson, A. L.: Secondary organic aerosol formation exceeds primary particulate matter emissions for light-duty gasoline vehicles, Atmospheric Chemistry and Physics, 14, 4661-4678, 10.5194/acp-14-4661-2014, 2014a.
Gordon, T. D., Presto, A. A., Nguyen, N. T., Robertson, W. H., Na, K., Sahay, K. N., Zhang, M., Maddox, C., Rieger, P., Chattopadhyay, S., Maldonado, H., Maricq, M. M., and Robinson, A. L.: Secondary organic aerosol production from diesel vehicle exhaust: impact of aftertreatment, fuel chemistry and driving cycle, Atmospheric Chemistry and Physics, 14, 4643-4659, 10.5194/acp-14-4643-2014, 2014b.
Guerreiro, C. B., Foltescu, V., and De Leeuw, F.: Air quality status and trends in Europe, Atmospheric environment, 98, 376-384, 2014.
Hak, C. S., Hallquist, M., Ljungstrom, E., Svane, M., and Pettersson, J. B. C.: A new approach to in-situ determination of roadside particle emission factors of individual vehicles under conventional driving conditions, Atmospheric Environment, 43, 2481-2488, 10.1016/j.atmosenv.2009.01.041, 2009.
Hallquist, A. M., Jerksjo, M., Fallgren, H., Westerlund, J., and Sjodin, A.: Particle and gaseous emissions from individual diesel and CNG buses, Atmospheric Chemistry and Physics, 13, 5337-5350, 10.5194/acp-13-5337-2013, 2013.
Hallquist, M., Wenger, J. C., Baltensperger, U., Rudich, Y., Simpson, D., Claeys, M., Dommen, J., Donahue, N., George, C., and Goldstein, A.: The formation, properties and impact of secondary organic aerosol: current and emerging issues, Atmospheric chemistry and physics, 9, 5155-5236, 2009.
Hao, L., Kari, E., Leskinen, A., Worsnop, D. R., and Virtanen, A.: Direct contribution of ammonia to< i> α</i>-pinene secondary organic aerosol formation, Atmospheric Chemistry and Physics, 20, 14393-14405, 2020.
Hassaneen, A., Munack, A., Ruschel, Y., Schroeder, O., and Krahl, J.: Fuel economy and emission characteristics of Gas-to-Liquid (GTL) and Rapeseed Methyl Ester (RME) as alternative fuels for diesel engines, Fuel, 97, 125-130, 2012.
Huang, M., Xu, J., Cai, S., Liu, X., Hu, C., Gu, X., Zhao, W., Fang, L., and Zhang, W.: Chemical analysis of particulate products of aged 1, 3, 5-trimethylbenzene secondary organic aerosol in the presence of ammonia, Atmospheric Pollution Research, 9, 146-155, 2018.
Janhäll, S., and Hallquist, M.: A novel method for determination of size-resolved, submicrometer particle traffic emission factors, Environmental Science & Technology, 39, 7609-7615, http://doi.org/10.1021/es048208y, 2005.
Jathar, S. H., Friedman, B., Galang, A. A., Link, M. F., Brophy, P., Volckens, J., Eluri, S., and Farmer, D. K.: Linking load, fuel, and emission controls to photochemical production of secondary organic aerosol from a diesel engine, Environmental science & technology, 51, 1377-1386, 2017a.
Jathar, S. H., Heppding, C., Link, M. F., Farmer, D. K., Akherati, A., Kleeman, M. J., de Gouw, J. A., Veres, P. R., and Roberts, J. M.: Investigating diesel engines as an atmospheric source of isocyanic acid in urban areas, Atmospheric Chemistry and Physics, 17, 8959-8970, 10.5194/acp-17-8959-2017, 2017b.
Jezek, I., Drinovec, L., Ferrero, L., Carriero, M., and Mocnik, G.: Determination of car on-road black carbon and particle number emission factors and comparison between mobile and stationary measurements, Atmospheric Measurement Techniques, 8, 43-55, 10.5194/amt-8-43-2015, 2015.
Kang, E., Root, M. J., Toohey, D. W., and Brune, W. H.: Introducing the concept of Potential Aerosol Mass (PAM), Atmospheric Chemistry and Physics, 7, 5727-5744, DOI 10.5194/acp-7-5727-2007, 2007.
Kawamura, K., Ng, L. L., and Kaplan, I. R.: Determination of organic acids (C1-C10) in the atmosphere, motor exhausts, and engine oils, Environmental science & technology, 19, 1082-1086, 1985.
Kawamura, K., and Kaplan, I. R.: Motor exhaust emissions as a primary source for dicarboxylic acids in Los Angeles ambient air, Environmental science & technology, 21, 105-110, 1987.
Kirchstetter, T. W., Harley, R. A., and Littlejohn, D.: Measurement of nitrous acid in motor vehicle exhaust, Environmental science & technology, 30, 2843-2849, 1996.
Kroll, J. H., Smith, J. D., Che, D. L., Kessler, S. H., Worsnop, D. R., and Wilson, K. R.: Measurement of fragmentation and functionalization pathways in the heterogeneous oxidation of oxidized organic aerosol, Physical Chemistry Chemical Physics, 11, 8005-8014, 2009.
Kuittinen, N., McCaffery, C., Peng, W., Zimmerman, S., Roth, P., Simonen, P., Karjalainen, P., Keskinen, J., Cocker, D. R., and Durbin, T. D.: Effects of driving conditions on secondary aerosol formation from a GDI vehicle using an oxidation flow reactor, Environmental Pollution, 282, 117069, 2021.
Kurtenbach, R., Becker, K., Gomes, J., Kleffmann, J., Lörzer, J., Spittler, M., Wiesen, P., Ackermann, R., Geyer, A., and Platt, U.: Investigations of emissions and heterogeneous formation of HONO in a road traffic tunnel, Atmospheric Environment, 35, 3385-3394, 2001.
Kwak, J. H., Kim, H. S., Lee, J. H., and Lee, S. H.: On-Road Chasing Measurement of Exhaust Particle Emissions from Diesel, Cng Lpg and Dme-Fueled Vehicles Using a Mobile Emission Laboratory, International Journal of Automotive Technology, 15, 543-551, http://doi.org/10.1007/s12239-014-0057-z, 2014.

Lambe, A., Ahern, A., Williams, L., Slowik, J., Wong, J., Abbatt, J., Brune, W., Ng, N., Wright, J., and Croasdale, D.: Characterization of aerosol photooxidation flow reactors: heterogeneous oxidation, secondary organic aerosol formation and cloud condensation nuclei activity measurements, Atmospheric Measurement Techniques, 4, 445-461, 2011.
Le Breton, M., Wang, Y., Hallquist, Å. M., Pathak, R. K., Zheng, J., Yang, Y., Shang, D., Glasius, M., Bannan, T. J., and Liu, Q.: Online gas-and particle-phase measurements of organosulfates, organosulfonates and nitrooxy organosulfates in Beijing utilizing a FIGAERO ToF-CIMS, Atmospheric Chemistry and Physics, 18, 10355-10371, 2018.
Le Breton, M., Psichoudaki, M., Hallquist, M., Watne, Å., Lutz, A., and Hallquist, Å.: Application of a FIGAERO ToF CIMS for on-line characterization of real-world fresh and aged particle emissions from buses, Aerosol Science and Technology, 53, 244-259, 2019.
Leslie, M. D., Ridoli, M., Murphy, J. G., and Borduas-Dedekind, N.: Isocyanic acid (HNCO) and its fate in the atmosphere: a review, Environmental Science: Processes & Impacts, 21, 793-808, 2019.
Li, T., Wang, Z., Yuan, B., Ye, C., Lin, Y., Wang, S., Yuan, Z., Zheng, J., and Shao, M.: Emissions of carboxylic acids, hydrogen cyanide (HCN) and isocyanic acid (HNCO) from vehicle exhaust, Atmospheric Environment, 247, 118218, 2021.
Liao, K., Chen, Q., Liu, Y., Li, Y. J., Lambe, A. T., Zhu, T., Huang, R.-J., Zheng, Y., Cheng, X., and Miao, R.: Secondary Organic Aerosol Formation of Fleet Vehicle Emissions in China: Potential Seasonality of Spatial Distributions, Environmental Science & Technology, 2021a.
Liao, K., Chen, Q., Liu, Y., Li, Y. J., Lambe, A. T., Zhu, T., Huang, R.-J., Zheng, Y., Cheng, X., and Miao, R.: Secondary organic aerosol formation of fleet vehicle emissions in China: Potential seasonality of spatial distributions, Environmental Science & Technology, 55, 7276-7286, 2021b.
Liao, S., Zhang, J., Yu, F., Zhu, M., Liu, J., Ou, J., Dong, H., Sha, Q., Zhong, Z., and Xie, Y.: High gaseous nitrous acid (HONO) emissions from light-duty diesel vehicles, Environmental science & technology, 55, 200-208, 2020.
Link, M. F., Friedman, B., Fulgham, R., Brophy, P., Galang, A., Jathar, S. H., Veres, P., Roberts, J. M., and Farmer, D. K.: Photochemical processing of diesel fuel emissions as a large secondary source of isocyanic acid (HNCO), Geophysical Research Letters, 43, 4033-4041, 10.1002/2016gl068207, 2016.
Liu, Q., Hallquist, Å. M., Fallgren, H., Jerksjö, M., Jutterström, S., Salberg, H., Hallquist, M., Le Breton, M., Pei, X., and Pathak, R. K.: Roadside assessment of a modern city bus fleet: Gaseous and particle emissions, Atmospheric Environment: X, 3, 100044, 2019a.
Liu, S., Thompson, S. L., Stark, H., Ziemann, P. J., and Jimenez, J. L.: Gas-phase carboxylic acids in a university classroom: Abundance, variability, and sources, Environmental Science & Technology, 51, 5454-5463, 2017.
Liu, T., Wang, X., Deng, W., Hu, Q., Ding, X., Zhang, Y., He, Q., Zhang, Z., Lu, S., Bi, X., Chen, J., and Yu, J.: Secondary organic aerosol formation from photochemical aging of light-duty gasoline vehicle exhausts in a smog chamber, Atmospheric Chemistry and Physics, 15, 9049-9062, 10.5194/acp-15-9049-2015, 2015.
Liu, T., Zhou, L., Liu, Q., Lee, B. P., Yao, D., Lu, H., Lyu, X., Guo, H., and Chan, C. K.: Secondary Organic Aerosol Formation from Urban Roadside Air in Hong Kong, Environ Sci Technol, 53, 3001-3009, 10.1021/acs.est.8b06587, 2019b.
Lopez-Hilfiker, F., Mohr, C., Ehn, M., Rubach, F., Kleist, E., Wildt, J., Mentel, T. F., Carrasquillo, A., Daumit, K., and Hunter, J.: Phase partitioning and volatility of secondary organic aerosol components formed from α-pinene ozonolysis and OH oxidation: the importance of accretion products and other low volatility compounds, Atmospheric chemistry and physics, 15, 7765-7776, 2015.
Lopez-Hilfiker, F. D., Mohr, C., Ehn, M., Rubach, F., Kleist, E., Wildt, J., Mentel, T. F., Lutz, A., Hallquist, M., Worsnop, D., and Thornton, J. A.: A novel method for online analysis of gas and particle composition: description and evaluation of a Filter Inlet for Gases and AEROsols (FIGAERO), Atmospheric Measurement Techniques, 7, 983-1001, 10.5194/amt-7-983-2014, 2014.
Martinet, S., Liu, Y., Louis, C., Tassel, P., Perret, P., Chaumond, A., and Andre, M.: Euro 6 unregulated pollutant characterization and statistical analysis of after-treatment device and driving-condition impact on recent passenger-car emissions, Environmental Science & Technology, 51, 5847-5855, 2017.
May, A. A., Nguyen, N. T., Presto, A. A., Gordon, T. D., Lipsky, E. M., Karve, M., Gutierrez, A., Robertson, W. H., Zhang, M., Brandow, C., Chang, O., Chen, S. Y., Cicero-Fernandez, P., Dinkins, L., Fuentes, M., Huang, S. M., Ling, R., Long, J., Maddox, C., Massetti, J., McCauley, E., Miguel, A., Na, K., Ong, R., Pang, Y. B., Rieger, P., Sax, T., Truong, T., Vo, T., Chattopadhyay, S., Maldonado, H., Maricq, M. M., and Robinson, A. L.: Gas- and particle-phase primary emissions from in-use, on-road gasoline and diesel vehicles, Atmospheric Environment, 88, 247-260, 10.1016/j.atmosenv.2014.01.046, 2014.
Millet, D. B., Baasandorj, M., Farmer, D. K., Thornton, J. A., Baumann, K., Brophy, P., Chaliyakunnel, S., de Gouw, J. A., Graus, M., and Hu, L.: A large and ubiquitous source of atmospheric formic acid, Atmospheric Chemistry and Physics, 15, 6283-6304, 2015.
Mohr, C., Lopez-Hilfiker, F. D., Yli-Juuti, T., Heitto, A., Lutz, A., Hallquist, M., D'Ambro, E. L., Rissanen, M. P., Hao, L., and Schobesberger, S.: Ambient observations of dimers from terpene oxidation in the gas phase: Implications for new particle formation and growth, Geophysical Research Letters, 44, 2958-2966, 2017.
Nakashima, Y., and Kondo, Y.: Nitrous acid (HONO) emission factors for diesel vehicles determined using a chassis dynamometer, Science of The Total Environment, 806, 150927, 2022.
Nam, E., Kishan, S., Baldauf, R. W., Fulper, C. R., Sabisch, M., and Warila, J.: Temperature effects on particulate matter emissions from light-duty, gasoline-powered motor vehicles, Environmental science & technology, 44, 4672-4677, 2010.
Nordin, E. Z., Eriksson, A. C., Roldin, P., Nilsson, P. T., Carlsson, J. E., Kajos, M. K., Hellen, H., Wittbom, C., Rissler, J., Londahl, J., Swietlicki, E., Svenningsson, B., Bohgard, M., Kulmala, M., Hallquist, M., and Pagels, J. H.: Secondary organic aerosol formation from

idling gasoline passenger vehicle emissions investigated in a smog chamber, Atmospheric Chemistry and Physics, 13, 6101-6116, 10.5194/acp-13-6101-2013, 2013.
Ortega, A. M., Hayes, P. L., Peng, Z., Palm, B. B., Hu, W., Day, D. A., Li, R., Cubison, M. J., Brune, W. H., and Graus, M.: Real-time measurements of secondary organic aerosol formation and aging from ambient air in an oxidation flow reactor in the Los Angeles area, Atmospheric Chemistry and Physics, 16, 7411-7433, 2016.
Palm, B. B., Campuzano-Jost, P., Ortega, A. M., Day, D. A., Kaser, L., Jud, W., Karl, T., Hansel, A., Hunter, J. F., and Cross, E. S.: In situ secondary organic aerosol formation from ambient pine forest air using an oxidation flow reactor, Atmospheric Chemistry and Physics, 16, 2943-2970, 2016.
Paulot, F., Wunch, D., Crounse, J. D., Toon, G., Millet, D. B., DeCarlo, P. F., Vigouroux, C., Deutscher, N. M., González Abad, G., and Notholt, J.: Importance of secondary sources in the atmospheric budgets of formic and acetic acids, Atmospheric Chemistry and Physics, 11, 1989-2013, 2011.
Pflaum, H., Hofmann, P., Geringer, B., and Weissel, W.: Potential of hydrogenated vegetable oil (HVO) in a modern diesel engine, SAE Technical Paper0148-7191, 2010.
Pirjola, L., Karl, M., Rönkkö, T., and Arnold, F.: Model studies of volatile diesel exhaust particle formation: are organic vapours involved in nucleation and growth?, Atmospheric Chemistry and Physics, 15, 10435-10452, 2015.
Pirjola, L., Dittrich, A., Niemi, J. V., Saarikoski, S., Timonen, H., Kuuluvainen, H., Jarvinen, A., Kousa, A., Ronkko, T., and Hillamo, R.: Physical and Chemical Characterization of Real-World Particle Number and Mass Emissions from City Buses in Finland, Environ Sci Technol, 50, 294-304, http://doi.org/10.1021/acs.est.5b04105, 2016.
Platt, S. M., El Haddad, I., Zardini, A. A., Clairotte, M., Astorga, C., Wolf, R., Slowik, J. G., Temime-Roussel, B., Marchand, N., Jezek, I., Drinovec, L., Mocnik, G., Mohler, O., Richter, R., Barmet, P., Bianchi, F., Baltensperger, U., and Prevot, A. S. H.: Secondary organic aerosol formation from gasoline vehicle emissions in a new mobile environmental reaction chamber, Atmospheric Chemistry and Physics, 13, 9141-9158, 10.5194/acp-13-9141-2013, 2013.
Preble, C. V., Dallmann, T. R., Kreisberg, N. M., Hering, S. V., Harley, R. A., and Kirchstetter, T. W.: Effects of Particle Filters and Selective Catalytic Reduction on Heavy-Duty Diesel Drayage Truck Emissions at the Port of Oakland, Environmental Science & Technology, 49, 8864-8871, 10.1021/acs.est.5b01117, 2015.
Ristimäki, J., Keskinen, J., Virtanen, A., Maricq, M., and Aakko, P.: Cold temperature PM emissions measurement: Method evaluation and application to light duty vehicles, Environmental science & technology, 39, 9424-9430, 2005.
Roberts, J. M., Veres, P. R., Cochran, A. K., Warneke, C., Burling, I. R., Yokelson, R. J., Lerner, B., Gilman, J. B., Kuster, W. C., and Fall, R.: Isocyanic acid in the atmosphere and its possible link to smoke-related health effects, Proceedings of the National Academy of Sciences, 108, 8966-8971, 2011.
Saliba, G., Saleh, R., Zhao, Y., Presto, A. A., Lambe, A. T., Frodin, B., Sardar, S., Maldonado, H., Maddox, C., and May, A. A.: Comparison of gasoline direct-injection (GDI) and port fuel injection (PFI) vehicle emissions: emission certification standards, cold-start, secondary organic aerosol formation potential, and potential climate impacts, Environmental science & technology, 51, 6542-6552, 2017.
Simonen, P., Saukko, E., Karjalainen, P., Timonen, H., Bloss, M., Aakko-Saksa, P., Rönkkö, T., Keskinen, J., and Dal Maso, M.: A new oxidation flow reactor for measuring secondary aerosol formation of rapidly changing emission sources, Atmospheric Measurement Techniques, 10, 1519-1537, 2017.
Suarez-Bertoa, R., and Astorga, C.: Isocyanic acid and ammonia in vehicle emissions, Transportation Research Part D: Transport and Environment, 49, 259-270, 2016.
Tkacik, D. S., Lambe, A. T., Jathar, S., Li, X., Presto, A. A., Zhao, Y. L., Blake, D., Meinardi, S., Jayne, J. T., Croteau, P. L., and Robinson, A. L.: Secondary Organic Aerosol Formation from in-Use Motor Vehicle Emissions Using a Potential Aerosol Mass Reactor, Environmental Science & Technology, 48, 11235-11242, 10.1021/es502239v, 2014.
Tong, Z., Li, Y., Lin, Q., Wang, H., Zhang, S., Wu, Y., and Zhang, K. M.: Uncertainty investigation of plume-chasing method for measuring on-road NOx emission factors of heavy-duty diesel vehicles, Journal of hazardous materials, 424, 127372, 2022.
Usmanov, R. A., Mazanov, S. V., Gabitova, A. R., Miftakhova, L. K., Gumerov, F. M., Musin, R. Z., and Abdulagatov, I. M.: The effect of fatty acid ethyl esters concentration on the kinematic viscosity of biodiesel fuel, Journal of Chemical & Engineering Data, 60, 3404-3413, 2015.
Vogt, R., Scheer, V., Casati, R., and Benter, T.: On-road measurement of particle emission in the exhaust plume of a diesel passenger car, Environmental science & technology, 37, 4070-4076, 2003.
Vourliotakis, G., and Platsakis, O.: ETC CM report 2022/02: Greenhouse gas intensities of transport fuels in the EU in 2020 - Monitoring under the Fuel Quality Directive, European Topic Centre on Climate change mitigation, 2022.
Wang, H., Wu, Y., Zhang, K. M., Zhang, S., Baldauf, R. W., Snow, R., Deshmukh, P., Zheng, X., He, L., and Hao, J.: Evaluating mobile monitoring of on-road emission factors by comparing concurrent PEMS measurements, Science of the Total Environment, 736, 139507, 2020.
Wang, J. M., Jeong, C.-H., Zimmerman, N., Healy, R. M., Hilker, N., and Evans, G. J.: Real-world emission of particles from vehicles: volatility and the effects of ambient temperature, Environmental Science & Technology, 51, 4081-4090, 2017.

Wang, Z., Nicholls, S. J., Rodriguez, E. R., Kummu, O., Hörkkö, S., Barnard, J., Reynolds, W. F., Topol, E. J., DiDonato, J. A., and Hazen, S. L.: Protein carbamylation links inflammation, smoking, uremia and atherogenesis, Nature medicine, 13, 1176-1184, 2007.
Watne, A. K., Psichoudaki, M., Ljungstrom, E., Le Breton, M., Hallquist, M., Jerksjo, M., Fallgren, H., Jutterstrom, S., and Hallquist, A. M.: Fresh and Oxidized Emissions from In-Use Transit Buses Running on Diesel, Biodiesel, and CNG, Environ Sci Technol, 52, 7720-7728, https://doi.org/10.1021/acs.est.8b01394, 2018.
Wentzell, J. J., Liggio, J., Li, S. M., Vlasenko, A., Staebler, R., Lu, G., Poitras, M. J., Chan, T., and Brook, J. R.: Measurements of gas phase acids in diesel exhaust: a relevant source of HNCO?, Environ Sci Technol, 47, 7663-7671, 10.1021/es401127j, 2013.
Yao, D., Guo, H., Lyu, X., Lu, H., and Huo, Y.: Secondary organic aerosol formation at an urban background site on the coastline of South China: Precursors and aging processes, Environmental Pollution, 309, 119778, 2022.
Yao, X., Fang, M., and Chan, C. K.: Size distributions and formation of dicarboxylic acids in atmospheric particles, Atmospheric Environment, 36, 2099-2107, 2002.
Yuan, B., Veres, P., Warneke, C., Roberts, J., Gilman, J., Koss, A., Edwards, P., Graus, M., Kuster, W., and Li, S.-M.: Investigation of secondary formation of formic acid: urban environment vs. oil and gas producing region, Atmospheric Chemistry and Physics, 15, 1975-1993, 2015.
Zervas, E., Montagne, X., and Lahaye, J.: C1− C5 organic acid emissions from an SI engine: Influence of fuel and air/fuel equivalence ratio, Environmental science & technology, 35, 2746-2751, 2001a.
Zervas, E., Montagne, X., and Lahaye, J.: Emission of specific pollutants from a compression ignition engine. Influence of fuel hydrotreatment and fuel/air equivalence ratio, Atmospheric Environment, 35, 1301-1306, 2001b.
Zhang, R., Suh, I., Zhao, J., Zhang, D., Fortner, E. C., Tie, X., Molina, L. T., and Molina, M. J.: Atmospheric new particle formation enhanced by organic acids, Science, 304, 1487-1490, 2004.
Zhao, Y., Saleh, R., Saliba, G., Presto, A. A., Gordon, T. D., Drozd, G. T., Goldstein, A. H., Donahue, N. M., and Robinson, A. L.: Reducing secondary organic aerosol formation from gasoline vehicle exhaust, Proceedings of the National Academy of Sciences, 114, 6984-6989, 2017.
Zhao, Y., Lambe, A. T., Saleh, R., Saliba, G., and Robinson, A. L.: Secondary Organic Aerosol Production from Gasoline Vehicle Exhaust: Effects of Engine Technology, Cold Start, and Emission Certification Standard, Environ Sci Technol, 52, 1253-1261, https://doi.org/10.1021/acs.est.7b05045, 2018.
Zhou, L., Hallquist, Å. M., Hallquist, M., Salvador, C. M., Gaita, S. M., Sjödin, Å., Jerksjö, M., Salberg, H., Wängberg, I., and Mellqvist, J.: A transition of atmospheric emissions of particles and gases from on-road heavy-duty trucks, Atmospheric Chemistry and Physics, 20, 1701-1722, 2020.
Zhou, L., Salvador, C. M., Priestley, M., Hallquist, M., Liu, Q., Chan, C. K., and Hallquist, Å. M.: Emissions and secondary formation of air pollutants from modern heavy-duty trucks in real-world traffic—chemical characteristics using on-line mass spectrometry, Environmental Science & Technology, 55, 14515-14525, 2021.